

THERMAL ANALYSIS OF BRIDGMAN - STOCKBARGER GROWTH

(NAS/ CR-1617.3) THERMAL ANALYSIS OF N79-20889
BRIDGMAN-STOCKBARGER GROWTH Final Technical
Report (Guests Associates, Inc., Huntsville,
Ala.) 98 p HC A05/MF A01 CSCL 20B
G3/76 19455
Unclas

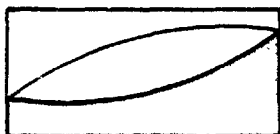
Final Technical Report

*Report No. AMD 79-TR1
March 15, 1979*

NAS 8-33204

Prepared for

**George C. Marshall Space Flight Center
National Aeronautics and Space Administration**



GAI

**ADVANCED MATERIALS DIVISION
HUNTSVILLE, ALABAMA 35805**



FINAL TECHNICAL REPORT
FOR
THERMAL ANALYSIS
OF
BRIDGMAN-STOCKBARGER GROWTH

15 March 1979

REPORT NO. AMD 79-TR1


Prepared for
GEORGE C. MARSHALL SPACE FLIGHT CENTER
NATIONAL AERONAUTICS AND SPACE ADMINISTRATION

Prepared by:

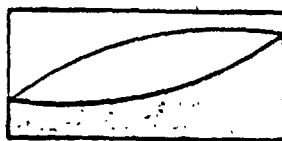


Frederick W. Knopf
Principal Investigator

Approved:



Fred K. Guest
President



GAI

ADVANCED MATERIALS DIVISION
HUNTSVILLE, ALABAMA 35805

TABLE OF CONTENTS

	<u>Title</u>	<u>Page No.</u>
LIST OF FIGURES		v
LIST OF TABLES		vii
1.0 INTRODUCTION AND SUMMARY		1-1
1.1 INTRODUCTION		1-1
1.2 STUDY APPROACH		1-3
1.3 SUMMARY OF RESULTS		1-4
1.4 STUDY RECOMMENDATIONS		1-7
2.0 DEFINITION OF THE BRIDGMAN-STOCKBARGER GROWTH CONFIGURATION		2-1
2.1 GROWTH OF HgCdTe SINGLE CRYSTALS		2-3
2.2 CONFIGURATION CHARACTERISTICS		2-5
2.2.1 <u>Experimenter-Controlled Parameters</u>		2-5
2.2.2 <u>Parameters Representing Physical Properties</u>		2-7
2.3 GROWTH ALTERNATIVES		2-7
3.0 BRIDGMAN-STOCKBARGER THERMAL ANALYSIS		3-1
3.1 CONSTANT SURFACE TEMPERATURE SPECIAL CASE ANALYSIS		3-2
3.2 PRELIMINARY CONFIGURATION ANALYSIS		3-7
3.3 TEMPERATURE BOOST GROWTH ALTERNATIVE		3-9
3.4 TEMPERATURE "DEBOOST" ANALYSIS		3-17
3.5 RADIATION COOLING EFFECTS		3-20
3.6 EFFECT OF AMPOULE DIMENSION VARIATIONS		3-23
3.7 THERMAL CONDUCTION EFFECTS		3-32
3.8 EFFECT OF GROWTH VELOCITY		3-41
4.0 REFERENCES		4-1

TABLE OF CONTENTS
(Continued)

	<u>Title</u>	<u>Page No.</u>
APPENDIX A:	SYSTEM THERMAL PROPERTIES.	A-1
A.1	PROPERTIES OF HgCdTe.	A-1
	A.1.1 <u>Thermal Conductivity</u>	A-1
	A.1.2 <u>Emissivity</u>	A-2
	A.1.3 <u>Thermal Diffusivity</u>	A-2
A.2	PROPERTIES OF FUSED SILICA.	A-4
	A.2.1 <u>Thermal Conductivity</u>	A-4
A.3	PROPERTIES OF THE THERMAL COUPLING AGENT BETWEEN THE CRUCIBLE AND THE FURNACE WALL	A-5
	A.3.1 <u>Thermal Conductivity</u>	A-5
APPENDIX B:	NUMERICAL SOLUTION TO THE THERMAL PROBLEM	B-1
B.1	THE DIFFERENTIAL EQUATION	B-1
B.2	FINITE DIFFERENCE EQUATIONS	B-3
B.3	TREATMENT OF BOUNDARY CONDITIONS.	B-7
	B.3.1 <u>Solid-Liquid Interface</u>	B-11
	B.3.2 <u>Sample/Crucible Interface (Sample Outer Surface)</u>	B-13
	B.3.3 <u>Crucible/Furnace Interface (Outer Crucible Wall)</u>	B-20
	B.3.4 <u>Inner Furnace Wall</u>	B-22
B.4	ITERATIVE PROCEDURE AND ACCURACY.	B-24

LIST OF FIGURES

<u>Figure No.</u>	<u>Title</u>	<u>Page</u>
2-1	Bridgman-Stockbarger Growth Environment	2-2
2-2	Phase Diagram for the HgCdTe System	2-4
3-1	Prescribed Sample Surface Temperature Boundary Condition	3-2
3-2	Thermal Profile and Gradient for the Constant Temperature Case	3-5
3-3	Temperature Profile Trend Away from the Interface	3-6
3-4	Thermal Profiles for the Constant Surface Temperature ($T_h=1000^\circ\text{C}$, $T_c=-270^\circ\text{C}$) Con- figuration	3-10
3-5	Isotherms for the $T_h=1000^\circ\text{C}$, $T_c=-270^\circ$ Con- figuration	3-11
3-6	Thermal Profiles for the Minimum Temperature Boost ($T_B=1300^\circ\text{C}$) Configuration	3-13
3-7	Thermal Profiles for the Maximum Temperature Boost ($T_B=2400^\circ\text{C}$) Configuration	3-14
3-8	Comparison of Thermal Profiles within the Constant Surface Temperature and Maximum Temperature Boost Configurations	3-16
3-9	Effect of Boosting the Inner Furnace Wall Temperature Near the Interface on the Ampoule Isotherms	3-18
3-10	Extractor Wall Temperature Requirements as a Function of Crucible Hot-Cold Temperature Differential	3-19
3-11	Extractor Temperature Effects on the Thermal Profiles for the Constant Hot-End Surface Temperature Configuration	3-21
3-12	Radiation Cooling Effects on the Ampoule Iso- therms	3-24
3-13	Effects of Sample Radius on the Ampoule Center- line Temperature Profile	3-25

LIST OF FIGURES (Continued)

<u>Figure No.</u>	<u>Title</u>	<u>Page</u>
3-14	Axial Thermal Gradient Trend for Variations in Sample Radius	3-26
3-15	Thermal Gradient - versus - Sample Radius Relationship	3-29
3-16	Isotherm Shifts for the Varying Radius Con- figurations	3-30
3-17	Effect of Changing Crucible Thickness-to- Sample Radius Ratio	3-31
3-18	Thermal Conduction Effects on the Ampoule Isotherms	3-35 3-36
3-19	Thermal Profiles for the Liquid Gallium Bath Growth Configuration (Cool End)	3-38
3-20	Effects of the Liquid Gallium Bath on the System Isotherms	3-39
3-21	Bridgman-Stockbarger Configurations Producing the Required 700°C Isotherm at the Mid- Plane Position	3-40
3-22	Effects of Growth Velocity on the Axial Thermal Gradient	3-42
3-23	Isotherm Movement as a Function of Growth Rate	3-44
B-1	Bridgman-Stockbarger Growth Environment	B-4
B-2	Boundary Conditions for the Bridgman-Stockbarger System	B-8
B-3	Prescribed Surface Temperature Boundary Conditions	B-9
B-4	Heat Conduction Boundary Condition	B-9
B-5	Radiation Boundary Condition	B-9
B-6	Schematic Heat Transfer Processes within the B-S Configuration	B-12
B-7	Spectral Radiancy Behavior as a Function of Wavelength and Temperature	B-16
B-8	Fused Silica Optical Transmission Characteristics	B-16
B-9	Fused Silica Transparency i ction as a Function of Temperature	B-19

1.0 INTRODUCTION AND SUMMARY

1.1 INTRODUCTION

NASA is currently conducting materials research directed toward the production of high quality tri-metal solid solution single crystals such as mercury cadmium telluride ($\text{Hg}_{1-x}\text{Cd}_x\text{Te}$) for use as infrared detectors. The program includes both experimentation in space (Spacelab Experiment No. MPS77F069) and ground based research to determine growth characteristics and configurations suitable for this class of materials. One of the primary growth requirements of solid solutions as compared to elemental and compound semiconductors is the necessity of extremely high thermal gradients at the growth interface to avoid constitutional supercooling. Growth configurations of the vertical Bridgman-Stockbarger type appear best suited to produce such high thermal gradients.

This report presents the results of a study in which a detailed thermal analysis of a cylindrical HgCdTe sample in a Bridgman-Stockbarger crystal growth configuration was conducted. The study concentrated on the thermal profile, interface shape and position, and the thermal gradients at the liquid-solid interface. This effort's analysis was based on alloys of HgTe and CdTe with compositions approximating 20% CdTe, 80% HgTe. This composition results in a bandgap suited for the detection of 10.6μ CO_2 radiation.

As part of the initial steps toward successful space growth

of HgCdTe, this analysis addressed the sensitivity of the sample thermal characteristics to important growth parameters, such as thermal diffusivities, thermal conductivities, furnace temperature profile, ampoule dimensions, and growth velocity. Physical properties of the different constituents as well as thermal characteristics are delineated in Appendix A. Alternate growth configurations were defined and evaluated to establish the Bridgman-Stockbarger system which best promotes optimum growth conditions.

Of primary interest in this study is the determination of the minimal thermal gradient over the growth interface as this determines stability in terms of constitutional supercooling. Throughout this report, this thermal gradient, located on the longitudinal axis of the sample at the growth interface in the direction of increasing temperature (into the liquid), will be referred to as the "thermal gradient" unless otherwise specified.

The study was carried out for HgCdTe contained in a fused silica crucible as this, to date, represents the only acceptable material from a chemical and structural standpoint.

Included in this study effort was the development of the numerical techniques and associated computational models necessary to analyze the heat transfer process within the sample and the Bridgman-Stockbarger boundary conditions. This thermal analysis model has been programmed in Fortran V, and is currently operational on the MSFC Univac 1100 system. Detailed descriptions of the thermal equations used in this analysis are presented in Appendix B.

1.2 STUDY APPROACH

As a first step to bound the thermal gradient achievable and to provide a test for the numerical computations, the so called "constant surface temperature" case was analyzed. This case considers an infinitely long cylinder of uniform thermal conductivity with upper half and lower half surface temperatures at fixed values of T_h and T_c respectively. Under these conditions, the problem can be solved analytically and yields under suitable restrictions the maximum thermal gradient achievable at the center of the sample and at the growth interface.

The next step was to consider the realistic configuration with the sample enclosed by a quartz crucible and various thermal couplings to a furnace wall. Parametric studies were carried out to determine the effects of the following:

- Crucible characteristics
- Thermal coupling to the furnace wall
- Thermal profiling in the hot end
- Cold end temperature
- Sample radius
- Crucible thickness
- Thermal conductivities
- Growth velocity

Specifically "the thermal gradient", interface shape, and interface thermal stability were studied as a function of the above variables leading to specific growth configurations which can in principle achieve the thermal characteristics required of the HgCdTe system.

This study led to the following three distinct growth configurations:

- Vacuum Coupling: The volume coupling the quartz crucible to the furnace wall is evacuated.
- Gas Coupling: The volume coupling the quartz crucible to the furnace wall is filled with a gas with conductivities ranging from 0.1 to 0.5 watt/meter-degree. This range encompasses the thermal conductivities for argon, nitrogen, and helium -- three suitable coupling agents.
- Liquid Metal Coupling: The volume coupling the quartz crucible to the furnace wall is filled with liquid Gallium on the cold end and either a vacuum or gas on the hot end.

The range of thermal gradients achievable with these configurations was established together with the interface shape and stability.

1.3 SUMMARY OF RESULTS

As indicated, the "constant surface temperature" case was analyzed with a detailed account given in a later section. The thermal gradient at the growth interface is given by

$$G = \frac{2}{3} \left[\frac{T_h - T_c}{R} \right]$$

where R is the sample radius. For the constant conductivity material in quartz with an interface temperature of $\sim 900^\circ\text{C}$, we have $T_h = 1000^\circ\text{C}$

(yield point of quartz) and $T_c = 400^\circ\text{C}$ (to obtain a 700°C interface temperature). Thus for a sample diameter of one centimeter, the gradient is

$$G = \frac{2}{3} \left[\frac{1000-400}{1/2} \right] = 800^\circ\text{C/cm}$$

It should be noted that this result is independent of the thermal conductivity of the sample so long as it is uniform. With the restrictions that the quartz does not exceed 1000°C and that the 700°C isotherm be flat, and not considering effects of different thermal conductivities of the solid and melt, this value represents the maximum achievable thermal gradient for a 1 cm diameter sample.

In all configurations studied, the effects of growth velocity for values of interest to the HgCdTe system were found to be inconsequential. In fact, as shown in detail later, growth velocities as high as 5 cm/hr produce no significant effect on the thermal gradient and only a 1% variation was found for growth rates as high as 10 cm/hr. In this summary, we do not further consider growth velocity as an instrumental parameter in the growth configuration.

All results present in this summary correspond to a hot end furnace wall temperature of 1000°C .

For the vacuum configuration, the following gradients were found for various sample radii:

R(mm)	Minimum Probable G($^\circ\text{C/cm}$)	Maximum Probable G($^\circ\text{C/cm}$)
6	263	315
5	300	450
4	349	496
3	422	548
2	533	670

The lower values represent the most unfavorable cases of thermal conductivities included by the uncertainties in present knowledge. Similarly, the larger G values represent the most favorable cases. It should be noted that an increase of up to 33% in gradient can be achieved by profiling the hot end temperature in the vacuum configuration. This effect, as expected, is not as pronounced in the other configurations.

In the gas configuration, the thermal coupling to the furnace wall is increased with a corresponding increase in thermal gradient. The following typical data is for nominal values of the conductivities and for a gas conductivity of $k_g = 0.5$ watt/meter-degree.

<u>R(mm)</u>	<u>G(°C/cm)</u>
5	507
4	643
2	1280

For lower gas conductivities, a substantial increase in G is realized over the vacuum case. For example, for $R=5$ mm and $k_g = 0.1$ watt/meter-degree, a gradient of 443°C/cm is realized.

The Ga configuration was studied both with vacuum and gas coupling on the hot end. The thermal gradients achieved, again for nominal values of the conductivities, for the Ga-vacuum case are as follows:

<u>R(mm)</u>	<u>G(°C/cm)</u>
5	404
4	484
2	670

We note that no significant increase is found, in fact, the gradients are not as high as the $k_g=0.5$ gas configuration. Increasing the thermal coupling on the hot end by the addition of gas results in the following for $R=5$ mm:

k_g (watts/meter-degree)	G ($^{\circ}\text{C}/\text{cm}$)
0	404
.5	647
1.0	705

In the Ga-vacuum case, the heat input from the 1000°C furnace wall is limiting the gradient achievable; an increase in thermal conductivity in the hot end allows the gradient to increase. For higher gradients, a method of providing higher hot end temperatures must be found. A growth configuration capable of accomplishing this is discussed in the next section.

1.4 STUDY RECOMMENDATIONS

From the above results, it appears possible to get HgCdTe crystal growth within the Bridgman-Stockbarger configuration. We have already noticed the significant increase in thermal gradient realized by incorporating a liquid metal solution in the extractor end to increase cool-end conduction and drive the sample isotherms up into the melt. If we now can alter the configuration on the hot end to drive these same isotherms back toward the cooler, extremely high thermal gradients will result in the vicinity of the growth interface.

This configuration includes a fused silica screen (or "sleeve") which has been inserted into the hot end of the furnace cavity to surround the HgCdTe sample and crucible. Because of the quartz transparency phenomenon (see Appendix B), (quartz is transparent to shorter wavelengths, opaque to longer wavelengths) the sleeve effectively screens out the longer wavelength radiation, such that the outer crucible surface is no longer heated by radiation. This implies that nearly all radiation from the furnace wall passes directly to the HgCdTe ingot. Additionally, a gas flow is introduced between the sleeve and the ampoule for a "localized" cooling effect. Finally, a very hot (e.g., 1400°C) wall temperature source is used to get copious short wavelength radiation.

In this configuration, the melt temperature rises substantially above the crucible strain point temperature at the inner crucible surface. However, the heat flow in the crucible wall is now radially outward -- from the radiation captured by the melt to the cooling gas. Because of this cooled outer surface, the external crucible temperatures are below the strain point temperature, giving mechanical strength to the ampoule. The sleeve is protected in much the same way by the gas along its inner surface. Because of the "greenhouse" effect imposed by the silica sleeve, temperatures will exist in the melt that are higher than the 1000°C rupture limit of the crucible.

Results from this study indicate that this greenhouse hot-end/gallium bath cool-end configuration will produce temperatures on either side of the interface that provide the required gradients to avoid interface breakdown within the HgCdTe solution. In addition, minor experimental adjustments (e.g., decreasing the

sample radius) might be made to the configuration to further improve the thermal characteristics within the sample.

Other configurations appear feasible to some degree. For small sample radii and small growth velocities, stable growth conditions can be produced in both a vacuum and gas-filled furnace cavity. It should be realized, however, that in actual furnace configurations, there will be some reductions in the thermal gradients computed in this study. With this in mind, a maximum sample radius of approximately 3 mm should be considered, if a reasonable growth rate and transient growth length are to be achieved. Vacuum configurations are clearly less favorable than those including a gas-filled cavity.

From the data presented in this study, it is clear that the system physical properties (conductivities, emissivities, etc.) are determining factors in the feasibility of a given configuration. Once these values are known with better precision, the computations performed in this study should be refined.

2.0 DEFINITION OF THE BRIDGMAN-STOCKBARGER GROWTH CONFIGURATION

The materials processing configuration addressed by this study is the growth of single crystals from the melt in a Bridgman-Stockbarger configuration. In vertical Bridgman-Stockbarger growth, the sample material is contained in a suitable crucible, and this ampoule (sample and crucible) is placed in a furnace which provides the desired profile. Figure 2-1 portrays the system under investigation. The sample, crucible, and furnace are designed to obtain the highest possible degree of cylindrical symmetry in order to effect an appropriate solid-liquid interface shape. In some cases, the sample is rotated to ensure better symmetry. Directional solidification results from: (a) the movement of the ampoule through the furnace cavity, (b) the movement of the furnace surrounding the fixed ampoule, or (c) changing the temperature profile with respect to time. The first two methods are equivalent for an ideal non-rotating system, while the third is equivalent to the first two only with certain thermal profiles, over a restricted segment of the sample, and, of course, with the proper time dependence.

In the following paragraphs, the Bridgman-Stockbarger crystal growth configuration under analysis in this study is described in more detail. This effort's analysis was based on the sample material consisting of solutions of the compounds Mercury Telluride (HgTe) and Cadmium Telluride (CdTe). Descriptions of the physical properties of these compounds are given in Appendix A.

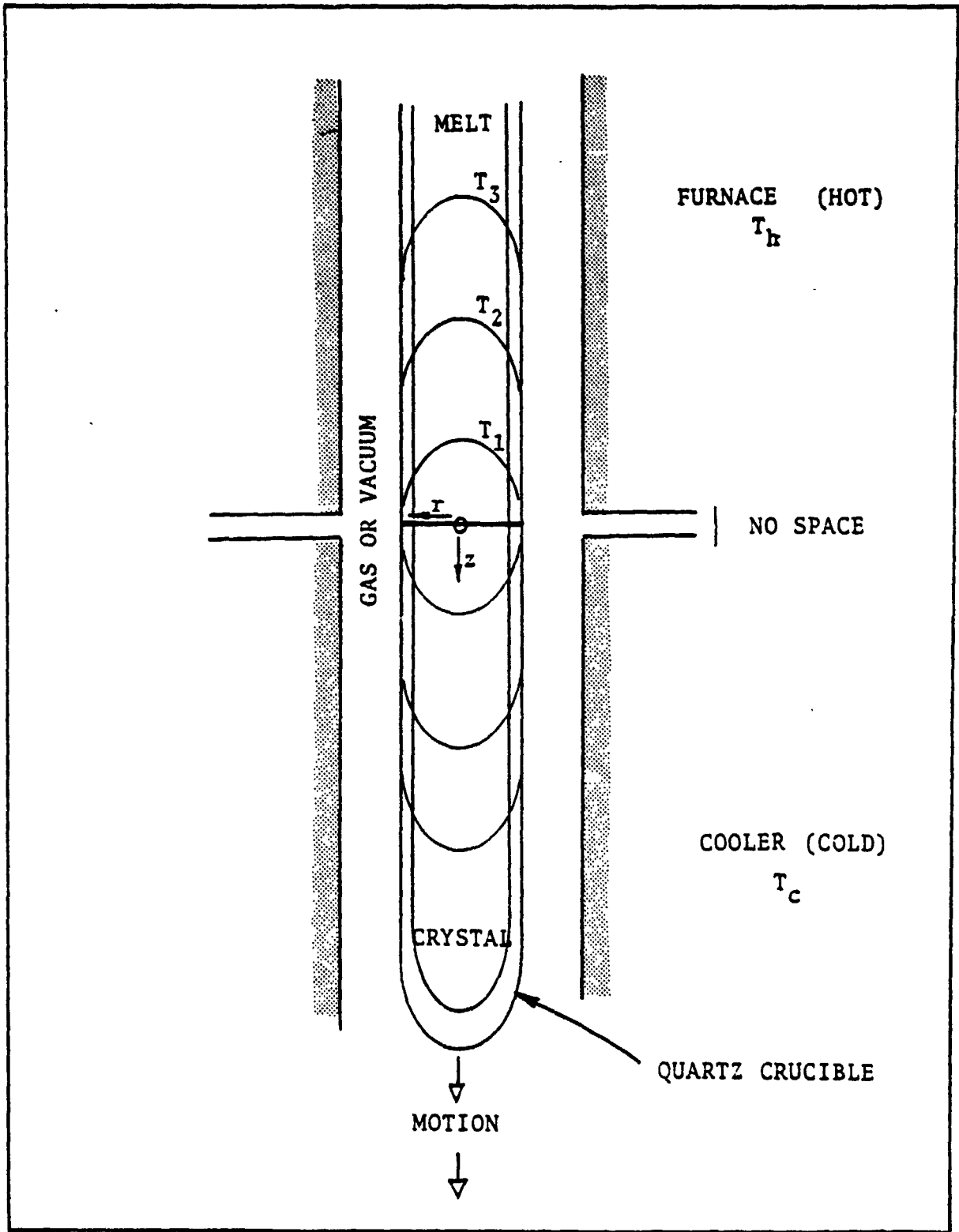


Figure 2-1 Bridgman-Stockbarger Growth Environment

2.1 GROWTH OF HgCdTe SINGLE CRYSTALS

In analyzing growth from the melt, this study is concerned with many aspects, including the type of material to be grown, the processing temperature and the containment of the molten material. In the case of HgCdTe, we are dealing with a mixture of a semimetal (HgTe) and a semiconductor (CdTe), with melting temperatures of 668°C and 1092°C, respectively.¹ The exact molar percentage of the constituents is usually specified by writing $\text{Hg}_{1-x}\text{Cd}_x\text{Te}$ ($0 \leq x \leq 1$) where, as indicated, the molar percentage of CdTe is 100x. Fused silica presently represents the only acceptable crucible material²; however, due to the high vapor pressure of Hg, this places a severe restriction on the maximum allowable temperature. Since this limits the achievable thermal gradients, growth rates in turn must be limited to avoid constitutional supercooling.

Taking the above-mentioned aspects into consideration, the growth conditions and the furnace characteristics necessary to achieve these conditions must be addressed. One of the major considerations is the thermal gradient at the growth interface necessary to avoid constitutional supercooling, which leads to interface breakdown. Constitutional supercooling is a form of supercooling caused by a change of solute-solvent ratio due to the preferred incorporation of one of the components in the solid.³ In the case of HgCdTe, this condition is severe, arising from the large separation of the liquidus and solidus curves. Noting the phase diagram of the HgCdTe system (Figure 2-2), we see that CdTe will be removed from the solidifying melt more rapidly than

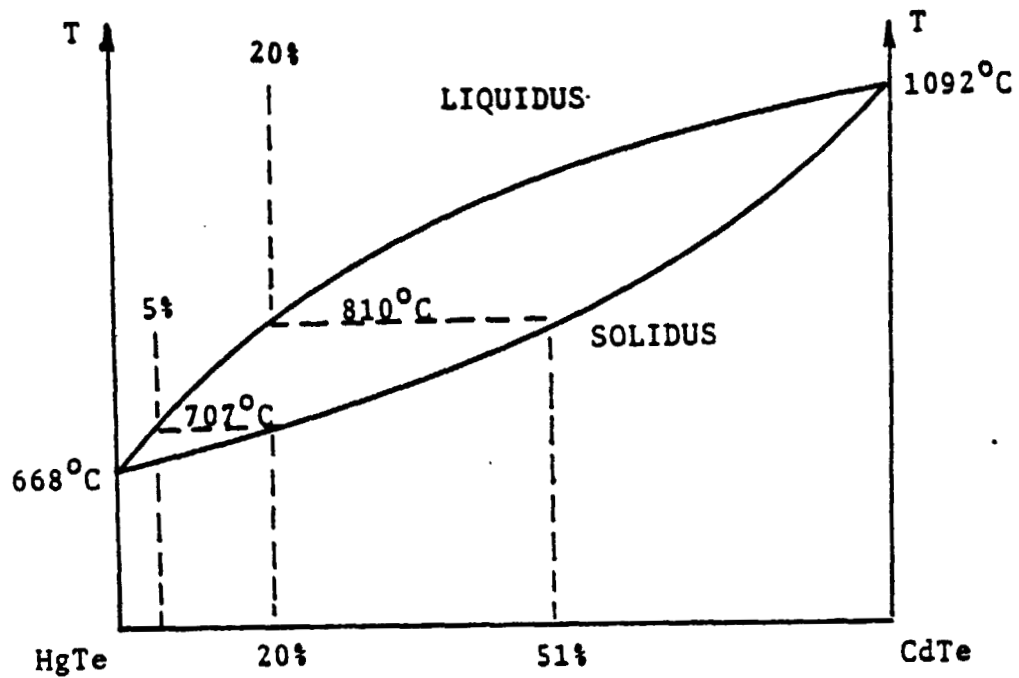


Figure 2-2 Phase Diagram for the HgCdTe System

the HgTe. This means that the melt at some distance removed from the interface will be richer in CdTe, and will therefore have a higher liquidus temperature. If the thermal gradient is not sufficient to assure a temperature above the liquidus, then some form of crystallization will be initiated in the liquid away from the interface. This effect is clearly aggravated by the high segregation coefficient, and may be suppressed only by maintaining a high thermal gradient or a slow growth rate. Rapid diffusion of CdTe in the melt helps, as it tends to maintain the concentration of that component constant up to the interface.

2.2 CONFIGURATION CHARACTERISTICS

Several experimenter-controlled parameters and physical/thermal material properties exist which are critical to determining realistic temperature profiles within the growth/melt of the Bridgman-Stockbarger configuration. As part of this study, a literature search of data relating to the B-S technique and fundamental data on the densities, specific heats, thermal conductivities, emissivities, etc. of HgCdTe and fused silica was completed and synopsized in the following paragraphs.

2.2.1 Experimenter-Controlled Parameters

The ampoule/furnace configuration for the Bridgman-Stockbarger technique was illustrated in Figure 2-1. Theoretically, there is an infinitely-thin insulated region in the furnace separating the hot and cool ends. Temperatures in the hot end can be expected to range from less than 1400°C (ferro-nickel furnace

elements) to 2500°C (tungsten elements in vacuum). Cool end temperatures in this study ranged from +200°C down to absolute zero (0°K, -273°C). Growth rates (i.e., ampoule or furnace movement) of from one-quarter to one centimeter per hour are realistic; however, growth velocity was parametrically analyzed in this study up to one meter per hour.

The physical dimensions of this system, also independent parameters in this study, are typically established relative to the size of the sample. To avoid the possibility of ampoule rupture of high temperatures (due to the high mercury vapor pressure), the thickness of the crucible is approximately 60% of the sample radius. A nominal sample diameter is 10 millimeters, making the fused silica thickness 3 millimeters. For this configuration, the furnace cavity may be 20 mm in diameter, leaving approximately 2 millimeters between the inner furnace wall and the outside of the crucible.

The length of the ampoule is not critical to this analysis. The behavior of the thermal profiles and gradients within the ampoule were evaluated in the region within five sample diameters on either side of the liquid-solid interface.

As was mentioned previously, fused silica presently represents the only acceptable crucible material for this crystal growth configuration at the high temperatures contemplated. However, silica too has its limitations, and must be restricted to less than 1000°C under the high vapor pressure of mercury, else rupture may occur. The optical transmission (i.e., radiation) characteristics of fused silica in the ultraviolet, visible

and infrared spectra are discussed in detail in Appendix B of this report.

2.2.2 Parameters Representing Physical Properties

Many of the parameters addressed in this thermal analysis represent physical properties of materials, and as such are not under the control of the experimenter. In some cases, these properties are not well known, or are somewhat variable from sample to sample (e.g., the thermal conductivity of fused silica). As such, it was useful in this analysis to treat these properties as if they were controllable to observe the effect of variation or uncertainty in these elements in the output thermal profile. Such an approach also extends the usefulness of the program to systems containing materials other than HgCdTe.

The physical properties of primary interest in the Bridgman-Stockbarger system describe the thermal characteristics of HgCdTe (the sample), fused silica (the crucible), and the coupling agent between the crucible outer surface and the furnace wall. These thermal properties include the thermal conductivities, emissivities, and diffusivities for the sample, crucible and coupling agent materials. A detailed discussion of these material properties is included for reference in Appendix A of this report; study assumptions regarding these properties are also presented.

2.3 GROWTH ALTERNATIVES

From the available configuration data, several interesting growth configurations have been established for detailed analysis

under this study. These configurations define different furnace, cooler, crucible and cavity arrangements for the crystal growth process. Inherent in these different configurations are a wide range of requirements relating to laboratory equipment, materials and hence cost.

The assumed baseline configuration is a uniform temperature heater with a uniform temperature heat extractor, with radiative coupling. The hot-end input power is limited to that which may produce quartz rupture temperatures of 1000°C or greater. Room temperature and refrigerated and heat extractors (down to 0°K) were considered for the cool end of the furnace cavity. The sensitivity of ingot thermal profiles and gradients to this cool-end temperature was investigated for temperatures ranging from -273°C to $+200^{\circ}\text{C}$.

Alternate heater end configurations were investigated in an attempt to optimize the thermal gradient at the liquid-solid interface. The maximum allowable quartz temperature limitation was enforced, but various temperature boosts near the interface on the heater end were specified, and the payoffs evaluated. By specifying several maximum temperatures at the interface with decaying thermal profiles along the heater wall such that at no point the outer crucible surface exceeded 1000°C , numerous state-of-the-art furnace configurations were modeled:

- Ferro-nickel (e.g., NICHROME, KANTHAL) heater elements -- providing up to 1400°C temperatures close to the interface. Possibly the least inexpensive furnace configuration for crystal growth.

- Platinum alloy (e.g., Pt-40% Rh) heater elements -- another inexpensive furnace design in which temperatures reaching 1800°C in air can be achieved with the platinum windings.
- Tungsten heater elements -- capable of achieving 2500°C in a vacuum; here, however, a quantum jump in cost is incurred because of the machinery associated with creating the vacuum.

Thermal analyses of these configurations were performed, and the payoffs in thermal gradients analyzed with system cost effectiveness in mind. If the relative increase in thermal gradient, with a consequent increase in crystal growth rate, does not justify the corresponding cost or complexity of the system configuration, then perhaps multiple systems producing an overall higher rate is the rational approach.

Other furnace-crucible arrangements were considered. The effect of sample radius (from 2 to 6 millimeters) within the same size furnace cavity was assessed. The crucible thickness-to-sample radius ratio was checked at 60% for all radii and, in addition, was reduced to as low as 33% for some samples.

Finally, for various hot and cold end temperature profiles, the furnace cavity was assumed to be filled with various gases (e.g., argon, dry nitrogen, helium), as well as evacuated. Thermal conductivities of the cavity medium were varied from 0 - 0.5 watt/meter-degree.

PRECEDING PAGE BLANK NOT FILMED

3.0 BRIDGMAN-STOCKBARGER THERMAL ANALYSIS

As the objectives of this study indicate, emphasis in this analysis was placed on investigating the behavior of the thermal profiles and gradients within an HgCdTe sample for selected Bridgman-Stockbarger growth configurations. Experimenter-controlled parameters (e.g., crucible dimensions, input temperature profiles) were analyzed parametrically to establish optimum growth configurations. In the following sections, the effects of the following variations in the B-S growth configuration will be presented:

- Alternate inner furnace wall temperature profiles -- at both the heater and extractor ends. Constant surface temperatures and boosted (and "deboosted") profiles were analyzed.
- Radiation cooling - vs - liquid bath cooling configurations.
- Ampoule (crucible/ingot) dimensions.
- Thermal conductivities of crucible, ingot (melt and solid), and ampoule surroundings.
- Growth velocity.

As part of this analysis, certain baseline configurations have been established which are used as a point of comparison to illustrate the effects of the parametric variations being considered. These baseline configurations are appropriately described in this section also.

Several special cases of the vertical B-S technique also were of interest to this study. These cases correspond to simplifications in the boundary conditions such that the system differential equation presented in Appendix B can be integrated analytically.

The analysis of one such case -- The Constant Surface Temperature Case -- is initially presented in this section to provide insight into the physical problem and to illustrate how the thermal profile is influenced by the physical parameters at the discretion of the experimenter. Results from this special case analysis were also used to corroborate the numerical techniques used to solve the non-integrable problems in this study.

3.1 CONSTANT SURFACE TEMPERATURE SPECIAL CASE ANALYSIS

To put the analysis of the Bridgman-Stockbarger growth configuration into proper perspective, simplifications in the system boundary conditions can be introduced to establish limits, trends, and deficiencies of the various growth configurations. The analytic solution of the Constant Surface Temperature Case is an example of the kind of solution which can be used.

Consider, as in Figure 3-1, the boundary condition

$T = T_c$ at $r = R$ for $z > 0$
 $T = T_h$ at $r = R$ for $z < 0$,
 where R is the sample radius.

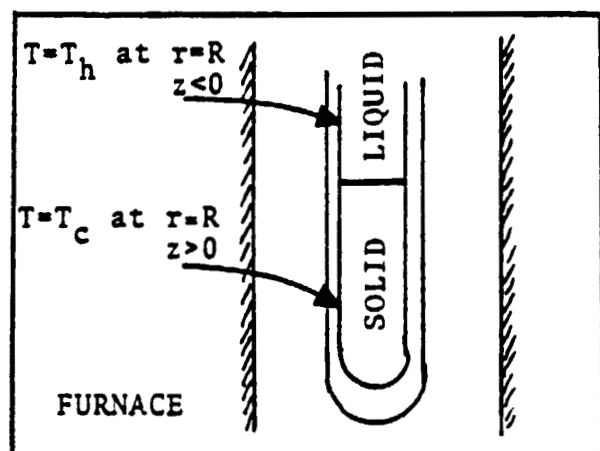


Figure 3-1. Prescribed Sample Surface Temperature Boundary Condition

This case approximates the conditions which produce a maximum thermal gradient at the solid-liquid interface with a maximum allowable temperature. Several aspects of this case are interesting. This problem for zero growth rate reduces to a solution of Laplace's equation with prescribed boundary temperatures. We first note that the thermal profiles are not dependent upon the thermal properties, provided the conductivity is given the same value at both ends of the sample. The solution is

$$\phi = \frac{T - T_c}{T_h - T_c} = \frac{1}{R} \sum_{n=1}^{\infty} \frac{J_0(r\alpha_n)}{\alpha_n J_1(R\alpha_n)} e^{-\alpha_n z}, \quad z > 0$$

$$\phi = 1 - \frac{1}{R} \sum_{n=1}^{\infty} \frac{J_0(r\alpha_n)}{\alpha_n J_1(R\alpha_n)} e^{+\alpha_n z}, \quad z < 0$$

where α_n are the positive roots of $J_0(R\alpha) = 0$. While these series provide a formal solution, certain problems arise. In the HgCdTe system, one of the most significant results is the minimum thermal gradient at the solid-liquid interface. If we attempt to compute this value, we note that the series

$$\frac{\partial \phi}{\partial z} (z = 0) = \frac{1}{R} \sum_{n=1}^{\infty} \frac{J_0(r\alpha_n)}{J_1(R\alpha_n)}$$

does not converge at $r = 0$. Therefore, this "standard textbook" solution is of little use to us in the region of most interest. However, it will provide, in the limit, an indication of the

maximum possible thermal gradient on axis at the interface as follows.

From the above normalized solutions, the range of ϕ is from 0 to 1, with the midplane value 0.5. The cylindrical coordinates are r and z , R is the crystal radius, and α_n is the n^{th} zero of J_0 . On the axis, $r = 0$ and $J_0(r=\alpha_n) = 1$. Figure 3-2 presents the axial temperature and thermal gradient for this constant surface temperature case with zero growth rate.

In the computer program that produced these results, the coordinates used are in units of R so that:

$$z' = z/R, \quad r' = r/R$$

and the on-axis function is

$$\phi(r'=0) = \sum_{n=1}^{\infty} \frac{1}{\alpha_n J_1(\alpha_n)} e^{-\alpha_n z'}$$

We expect that at $z' = 0$, $\phi = 0.5$, since continuity requires that the two equations for ϕ must yield the same result; therefore, $\phi(z'=0) = 1 - \phi(z'=0)$. The fact that the computer does not produce this result is due to the singular behavior of the series near $z'=0$. For all other values of z' , $\phi(z'=a) = 1 - \phi(z'=-a)$. Figure 3-3 illustrates the behavior of ϕ for larger values of z' , indicating that $\phi \rightarrow 1$ when the axial distance from the interface is approximately three times the crystal radius.

The gradient of ϕ is taken by dividing the difference between successive values of ϕ by the increment in z' . Since the values of ϕ nearest $z'=0$ are in error, the gradient of ϕ is likewise in error at that point, and, in fact, its sign appears reversed.

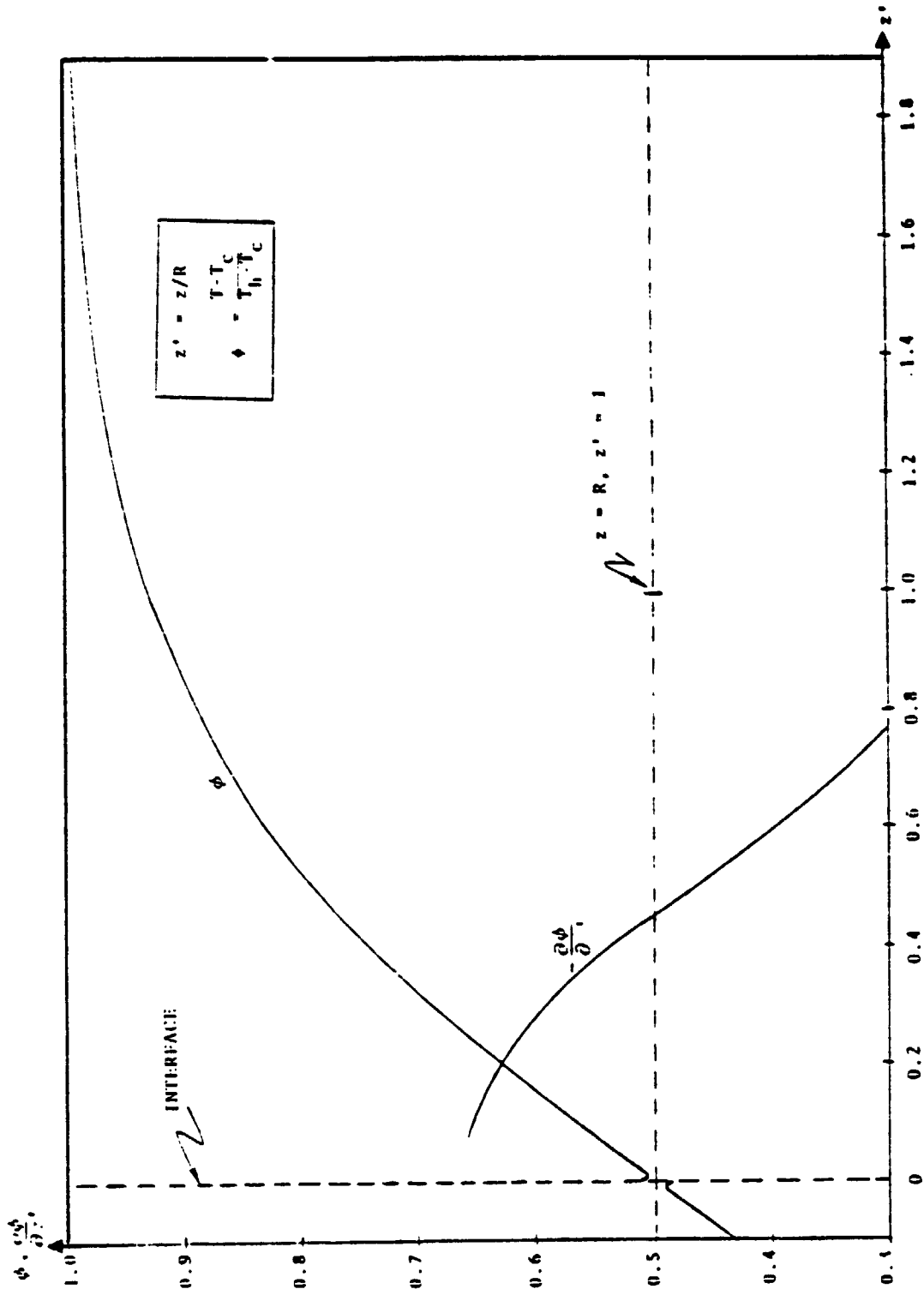


Figure 3-2 Thermal Profile and Gradient for the Constant Temperature Case

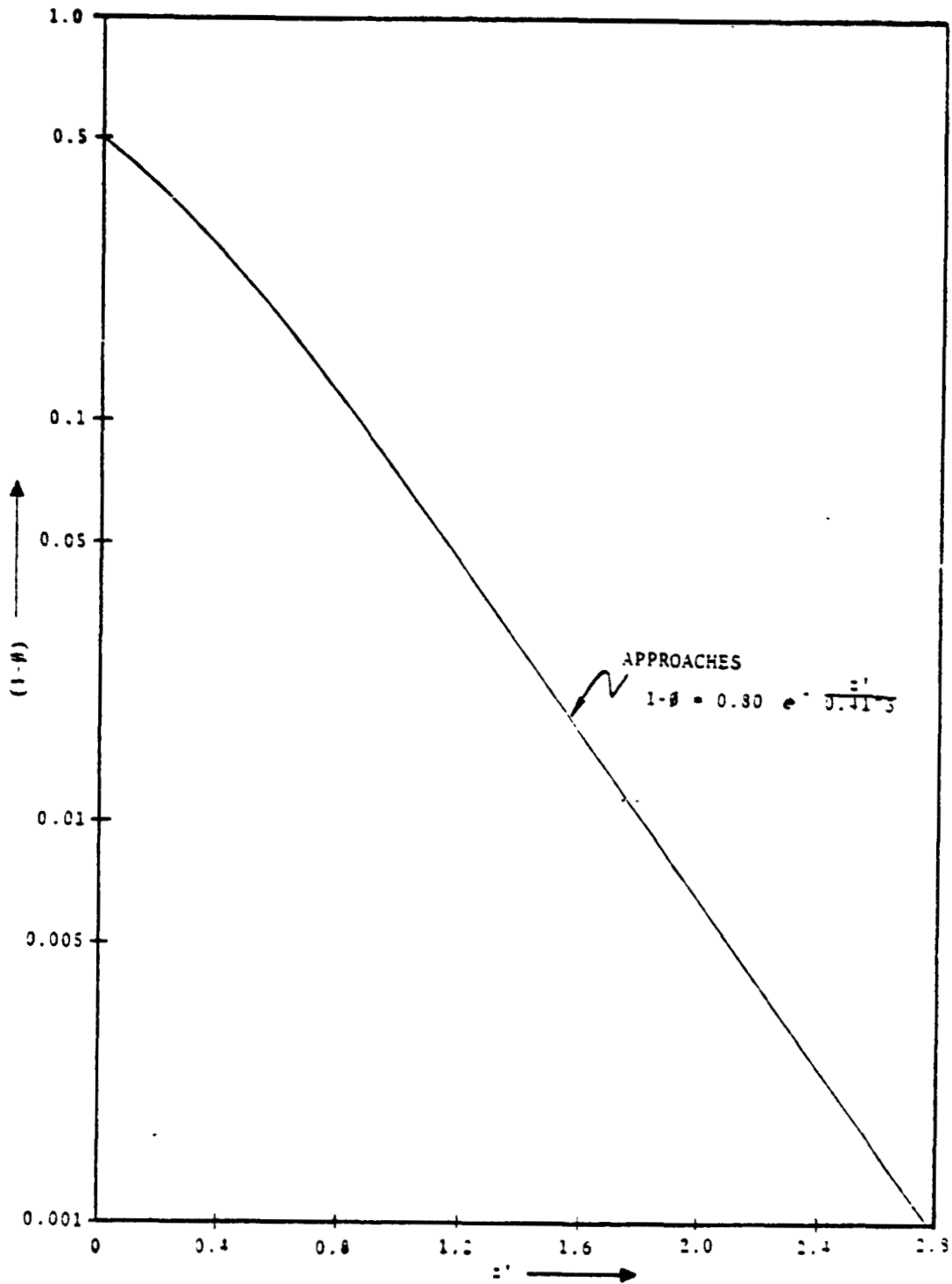


Figure 3-3 Temperature Profile Trend Away from the Interface

This is purely an artifact of the computation and illustrates the necessity of a careful examination of the convergence of such series representations. It appears that $\frac{\partial \phi}{\partial z}$, approaches the value $2/3$ at the origin, and that this then represents the limiting value of the gradient. This limit cannot be reached in real cases, as any real boundary conditions will be less favorable than these fictitious idealized ones.

In practical terms, if $T_h = 1000^\circ\text{C}$, limited by the mechanical properties of fused silica, and if the solidus temperature is 700°C (the mid-plane temperature), then $T_c = 400^\circ\text{C}$. Thus, $T_h - T_c = 600^\circ\text{C}$, and for $R = 1/2$ cm

$$\frac{\partial T}{\partial z} = \left[\frac{T_h - T_c}{R} \right] * \frac{\partial \phi}{\partial z} = \left(\frac{600}{1/2} \right) \left(\frac{2}{3} \right) = \frac{800^\circ\text{C}}{\text{cm}}$$

Thus, 800°C divided by the crystal diameter appears to be an absolute limit on the achievable minimum gradient. The most general expression would be

$$\frac{\partial T}{\partial z} \leq \frac{8}{3} \left[\frac{T_h - T_m}{d} \right],$$

where T_m is the midplane temperature and d is the diameter of the specimen.

3.2 PRELIMINARY CONFIGURATION ANALYSIS

Consider again the Bridgman-Stockbarger growth environment of Figure 2-1. The initial growth configuration considered by this analysis was a constant surface temperature profile for

both the inner furnace and cooler walls. The hot end temperature was specified to be 1000°C (limited by the high vapor pressures of mercury and the mechanical properties of fused silica). The extractor wall was specified to be -270°C (approximately absolute zero) to maximize the thermal gradient at the liquid/solid interface for this configuration. (One must recognize the experiment cost implications associated with this cooler configuration, however, when assessing the payoffs of this imposed external temperature gradient. As this analysis will indicate, heat extractor temperatures below -100°C have little influence on the system performance.)

For this configuration, the following additional specifications were selected:

- Thermal Conductivities

Fused silica : 2.5 watts/m°C¹
Sample (liquid): 1.0 watt/m°C
Sample (solid): 1.0 watt/m°C

(These conductivity values are later varied parametrically to assess their individual effects on growth conditions. For this preliminary configuration, equal conductivities for the melt and solid were assumed to force the thermal gradient immediately on either side of the liquid-solid interface to be equal.)

- Ampoule Dimensions

Sample ingot : 1 cm diameter
Crucible thickness: 60% of sample radius, or 3 mm.

- Emissivities

Fused silica: 1.0
Furnace : 1.0
Sample : 0.3

¹ See Appendix A

In addition, the furnace cavity is evacuated; that is, there is no conduction between this surface and the furnace wall. Finally, there is no ampoule motion, i.e., the growth velocity is zero.

Figure 3-4 presents the thermal characteristics within the sample for this described configuration. The temperature profile along both the outer crucible wall and the sample centerline (axis) are presented, as well as the axial thermal gradient. Note that the outer crucible temperature falls away from the 1000°C steady state value closer to the liquid-solid interface, indicating that a temperature boost in the heater end near the interface may be possible without jeopardizing crucible strength. This temperature boost may drive the maximum achievable gradient at the interface higher than the indicated 306°C/cm for this configuration.

Figure 3-5 presents the isotherms in the ampoule for this configuration. These isotherms remain relatively flat for approximately 100°C on either side of the HgCdTe solidus temperature of 700°C, promoting good crystal growth conditions at the interface for high thermal gradients.

3.5 TEMPERATURE BOOST GROWTH ALTERNATIVE

As the previous configuration analysis indicated, increased thermal gradients may be achieved by boosting the temperatures of the inner furnace wall near the interface. This configuration will yield an exponential temperature decay from a maximum temperature (near the interface) to the steady state temperature of 1000°C away from the interface. The form of this temperature profile (normalized) is (See Appendix B):

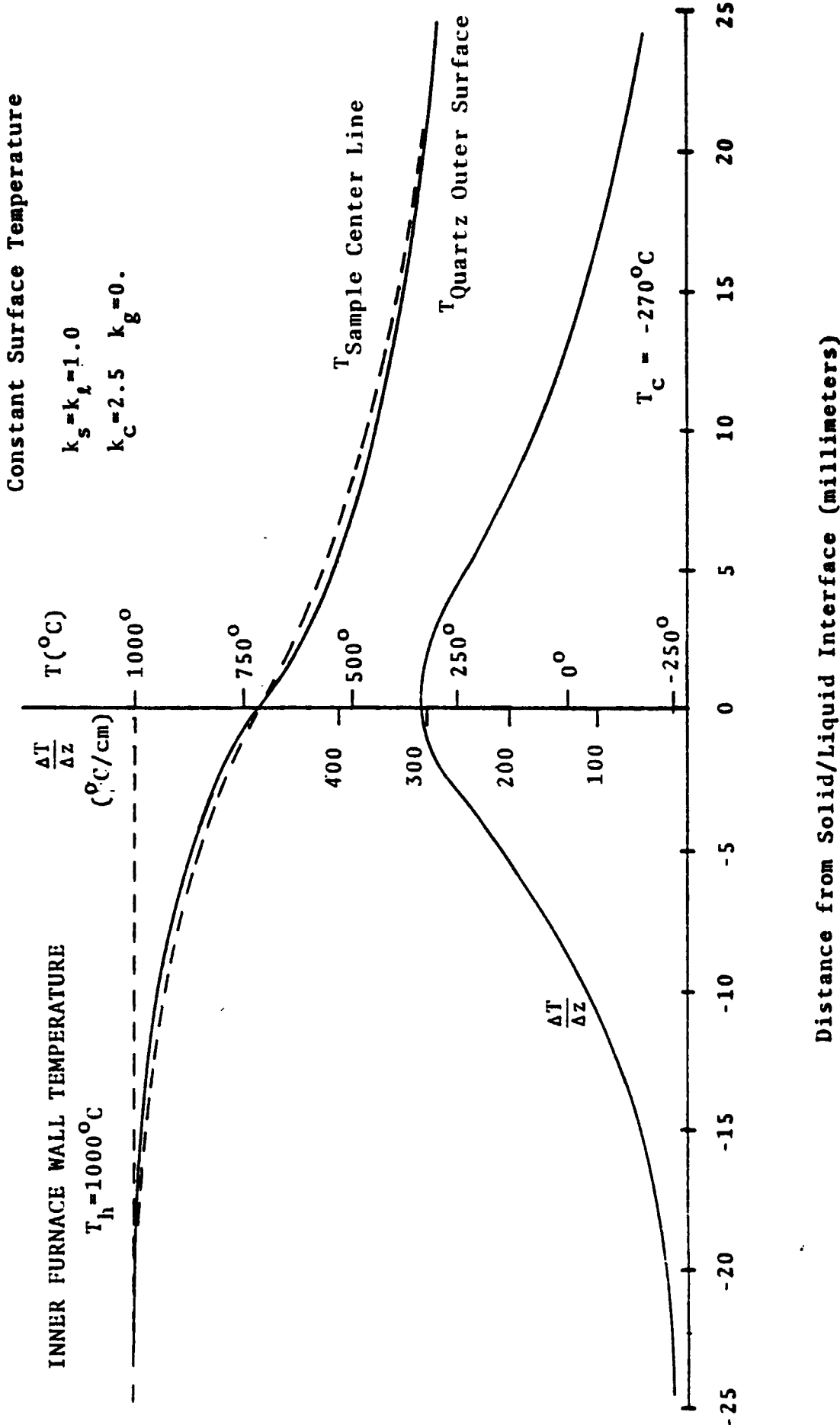


Figure 3-4 Thermal Profiles for the Constant Surface Temperature
 $(T_h = 1000^\circ\text{C}, T_C = -270^\circ\text{C})$ Configuration

Constant Surface Temperature

$$T_h = 1000^\circ\text{C}$$

$$T_c = -270^\circ\text{C}$$

$$k_s = k_l = 1.0 \quad k_c = 2.5 \quad k_g = 0.$$

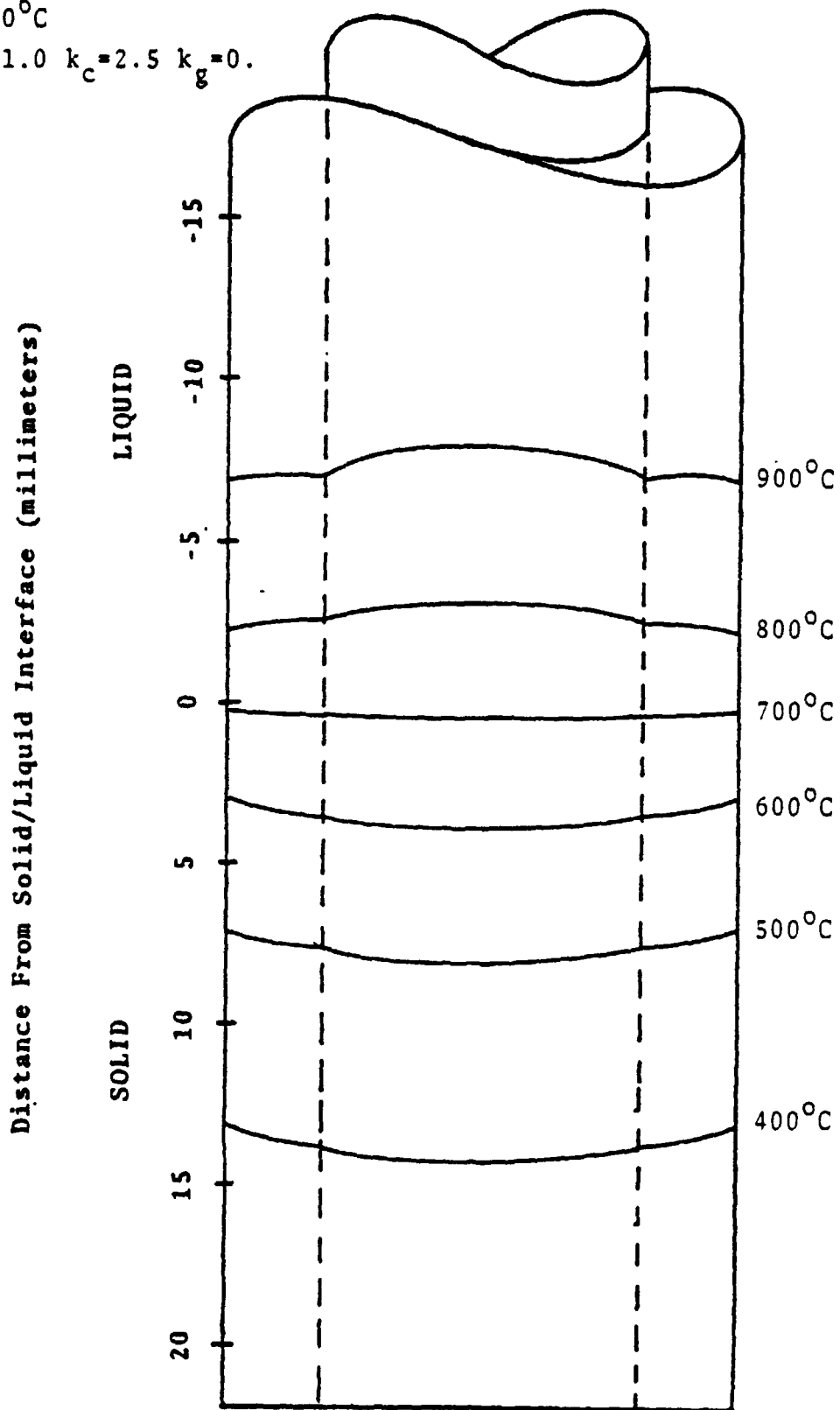


Figure 3-5 Isotherms for the $T_h = 1000^\circ\text{C}$, $T_c = -270^\circ$ Configuration

$$\phi_{\text{WALL}} = f(z) = 1. + Ae^{Bz} \quad (z < 0)$$

where A and B are constants representing the maximum temperature and temperature decay rate, respectively.

For this analysis, boost temperatures from 1300° to 2400°C were considered. This range is representative of furnace configurations utilizing heating elements of ferro-nickel (1200-1500°C), platinum-alloy (1600°-1800° in air), and tungsten (up to 2500° in vacuum) composition. For each temperature case, various decay rates (i.e., values of B) were investigated to determine the "critical value" of B such that the temperature profile on the outer crucible surface approached (but nowhere exceeded) the constant surface temperature limitations of 1000°C. Figures 3-6 and 3-7 present the thermal profiles for the minimum and maximum TBOOST temperatures considered -- 1300°C and 2400°C, respectively. The trend of outer crucible temperature for varying decay rates is evident in either case. Also illustrated is the axial thermal gradient for the "critical" decay rate, the optimum gradient achievable for each TBOOST configuration under the physical limitations imposed by the crucible.

Table 3.1 presents the maximum thermal gradients achieved for all temperature boost cases analyzed. Note that up to 30% increase in gradient (close to 400°C/cm) is realized over the previous constant surface temperature case. However, as the table indicates, this payoff is limited; as the maximum temperature is further increased, the maximum gradient moves away from the interface and begins to decrease. Figure 3-8 illustrates this trend as it compares the T = 2400°C boost thermal profiles with

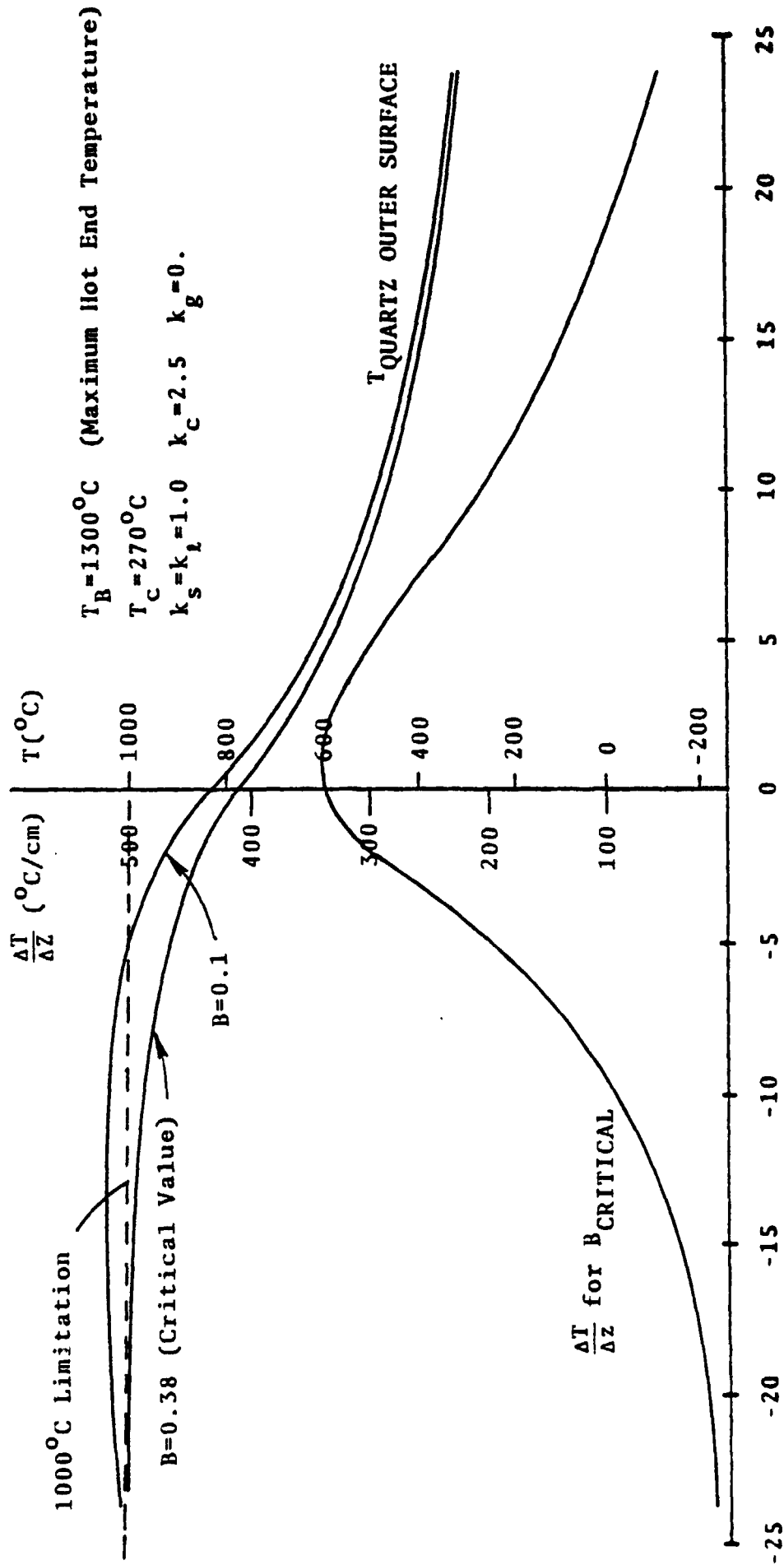
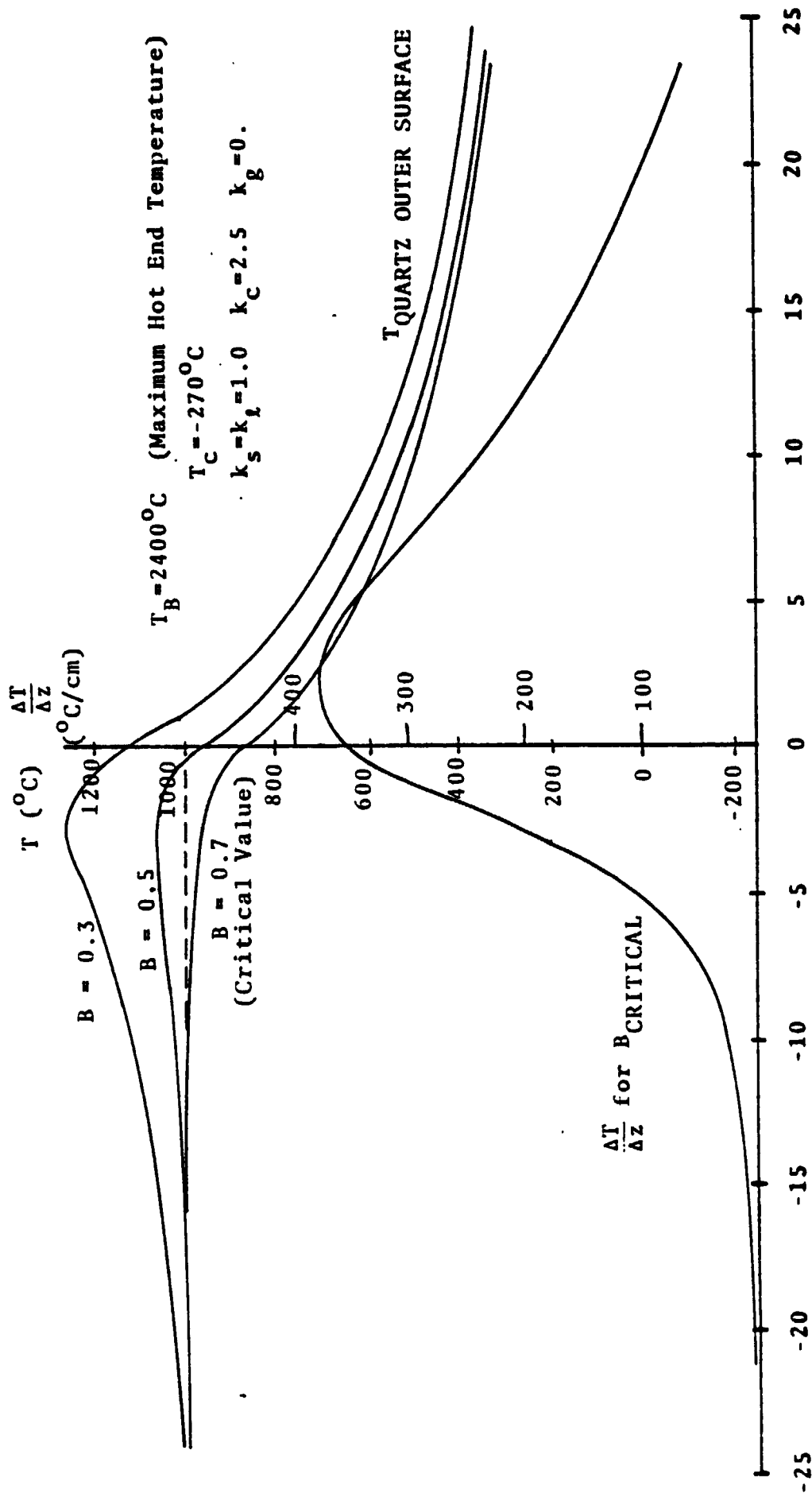


Figure 3-6 Thermal Profiles for the Minimum Temperature Boost ($T_B = 1300^\circ\text{C}$) Configuration



Distance from Solid/Liquid Interface (millimeters)

Figure 3-7 Thermal Profiles for the Maximum Temperature Boost
 ($T_B = 2400^\circ\text{C}$) Configuration

TABLE 3.1 TEMPERATURE BOOST EFFECTS

T_B ($^{\circ}\text{C}$)	A	B_{CRITICAL}	MAXIMUM AXIAL GRADIENT, $\Delta T/\Delta Z$ ($^{\circ}\text{C}/\text{cm}$)
1300	0.23566	0.40	340
1600	0.47133	0.40	350
1800	0.62844	0.40	380
2000	0.78555	0.45	395
2400	1.09976	0.70	380

Note: T_B = Maximum Boost Temperature along Inner Furnace Wall

$$T_B = (T_h - T_c) * \phi_B + T_c$$

where $\phi_B = 1. + Ae^{-Bz}$ (Normalized)

z = Distance away from Liquid-Solid Interface

T_c = Cool End Temperature = -270°C

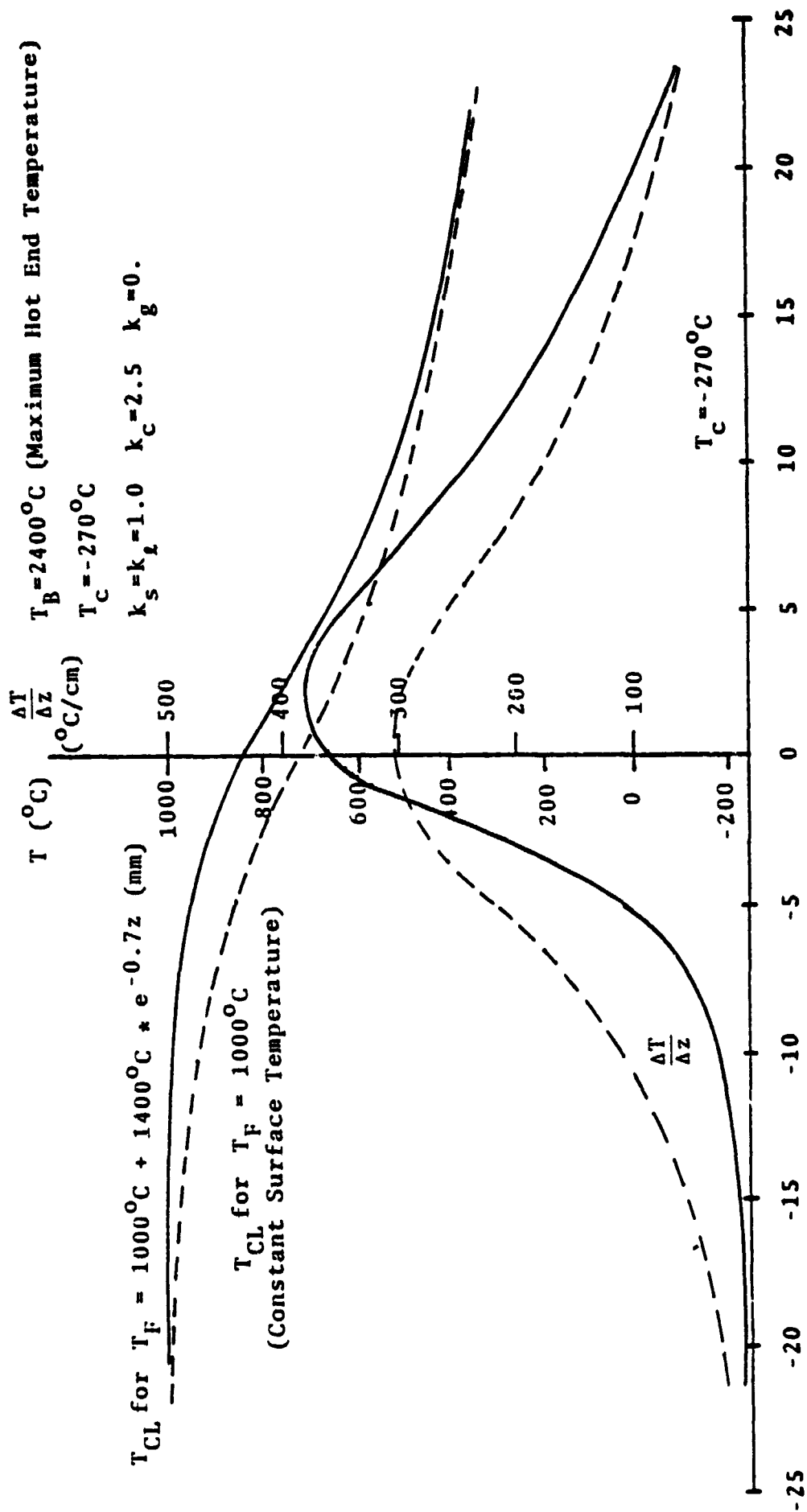


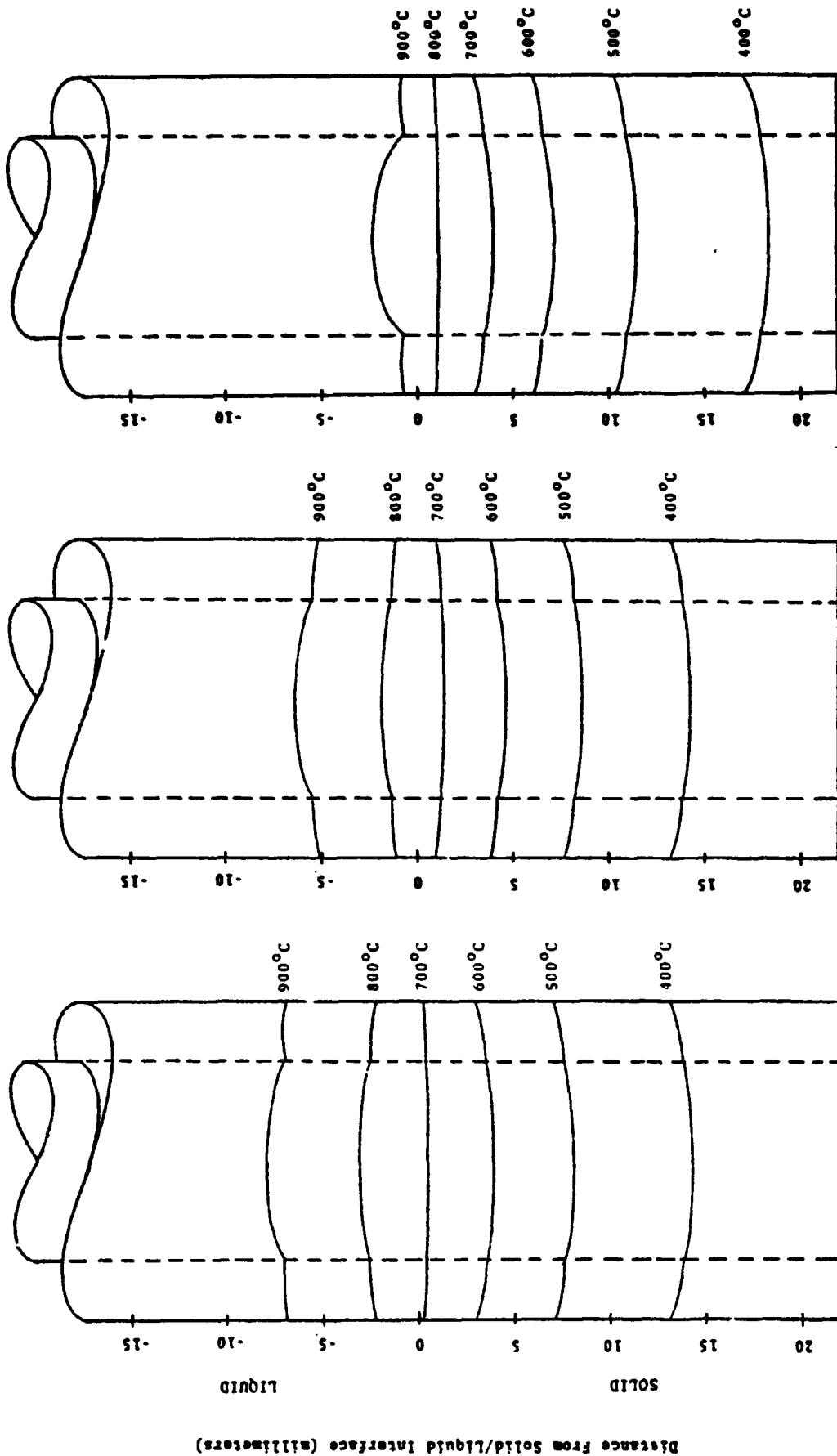
Figure 3-8 Comparison of Thermal Profiles within the Constant Surface Temperature and Maximum Temperature Boost Configurations

the constant surface temperature data presented previously.

Figure 3-9 illustrates the effect of boosting the inner furnace wall temperature near the interface on the ampoule isotherms. Isotherms for the TMAX = 1000° (constant temperature case), 1300°, and 2400°C are compared. The movement of isotherms toward the interface and into the solid end is evident. In all cases, the isotherms in the 600°-800°C temperature range remain relatively flat.

3.4 TEMPERATURE "DEBOOST" ANALYSIS

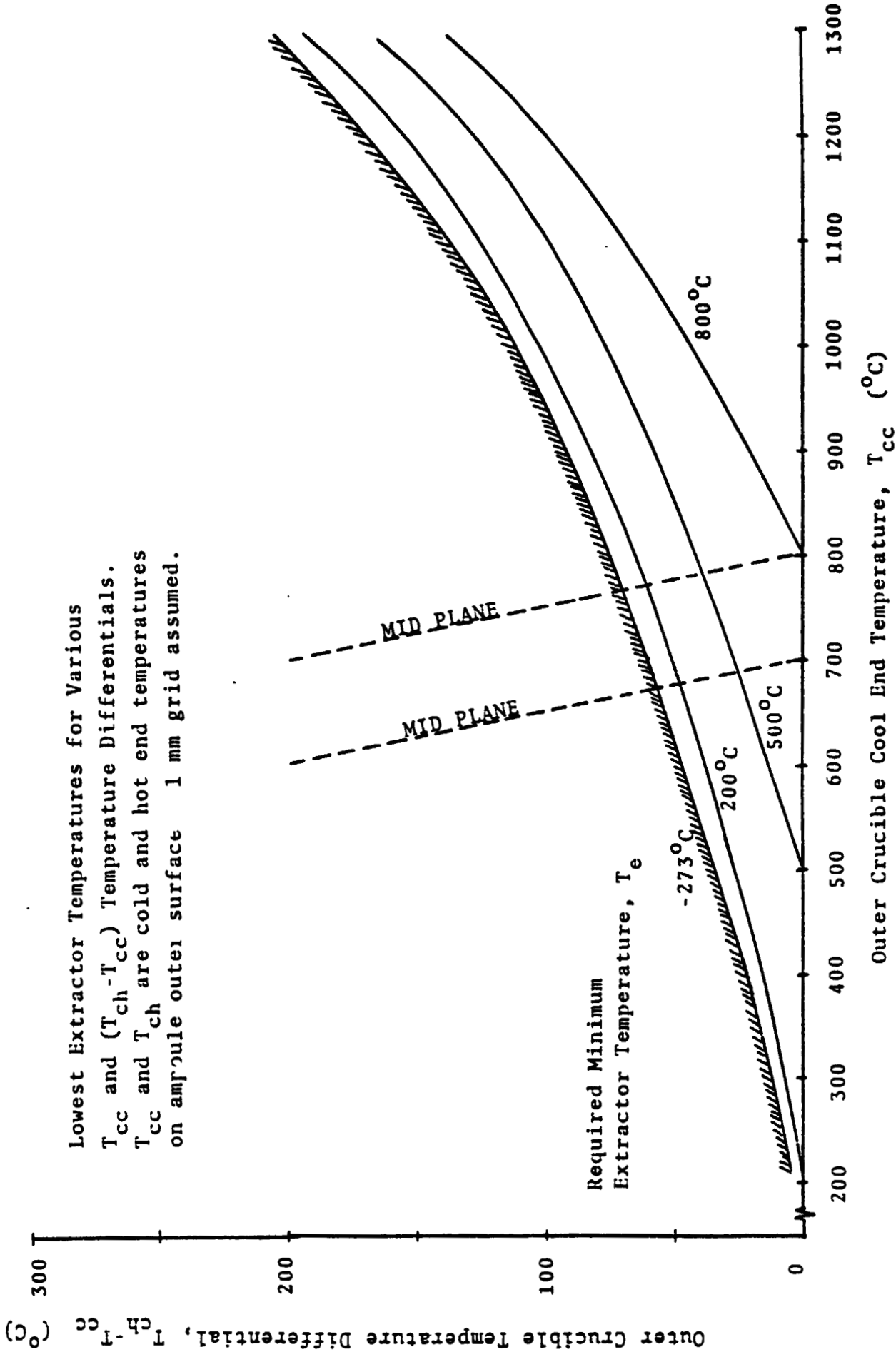
A similar thermal analysis was performed for the cool end of the configuration to establish the extractor wall requirements as a function of temperature differential (hot end - vs - cold end) for the quartz outer surface. Figure 3-10 presents lines of constant minimum extractor temperatures required to support the outer crucible temperature difference $T_{ch} - T_{cc}$ for various T_{cc} 's. Configuration temperatures were varied around the approximate growth faces expected for HgCdTe (700-800°C). As an example, if the hot end quartz surface temperature is ideally 1000°C (constant), the extractor would be able to withdraw only enough heat within one millimeter from the interface to lower the quartz temperature to 905°C -- and it would take a 0°K temperature at the extractor wall to achieve this reduction. Similarly, if the cool-end quartz temperature is 600°C, the best temperature differential along the quartz that the extractor can support is 50°C. Relaxing the extractor wall requirements to more reasonable (i.e., warmer) temperatures drives T_{ch} down for a specified T_{cc} or, for a specified $T_{ch} - T_{cc}$, drives both T_{cc} and T_{hc} higher.



a) No Boost ($T_h = 1000^\circ\text{C}$) b) $T_B = 1300^\circ\text{C}$ c) $T_B = 2400^\circ\text{C}$

$$T_C = -270^\circ\text{C} \quad k_S = k_L = 1.0 \quad k_C = 2.5 \quad k_g = 0.$$

Figure 3-9 Effect of Boosting the Inner Furnace Wall Temperature Near the Interface on the Ampoule Isotherms



Lowest Extractor Temperatures for Various T_{cc} and $(T_{ch} - T_{cc})$ Temperature Differentials. T_{cc} and T_{ch} are cold and hot end temperatures on ampoule outer surface 1 mm grid assumed.

Figure 3-10 Extractor Wall Temperature Requirements as a Function of Crucible Hot-Cold Temperature Differential

Of particular interest is the almost insignificant temperature differential gained (less than 10°C for almost all T_{cc}) by lowering the minimum extractor temperature from $+200^{\circ}\text{C}$ to 0°K (absolute zero) -- a range in temperature which has definite cost implications on extractor design. This data implies that the temperature profiles are insensitive to radiative-cooled extractor temperatures. These radiation-cooling effects are analyzed in more detail in the next section.

3.5 RADIATION COOLING EFFECTS

To further investigate the effects of the radiative-cooled furnace configuration, we considered both the 1000°C (constant) and temperature-boosted ($T_{MAX}=1300^{\circ}\text{C}$) hot-end furnace profiles with variable constant extractor temperatures ranging from $+200^{\circ}$ to -200°C . (The absolute zero temperature cases were discussed earlier.)

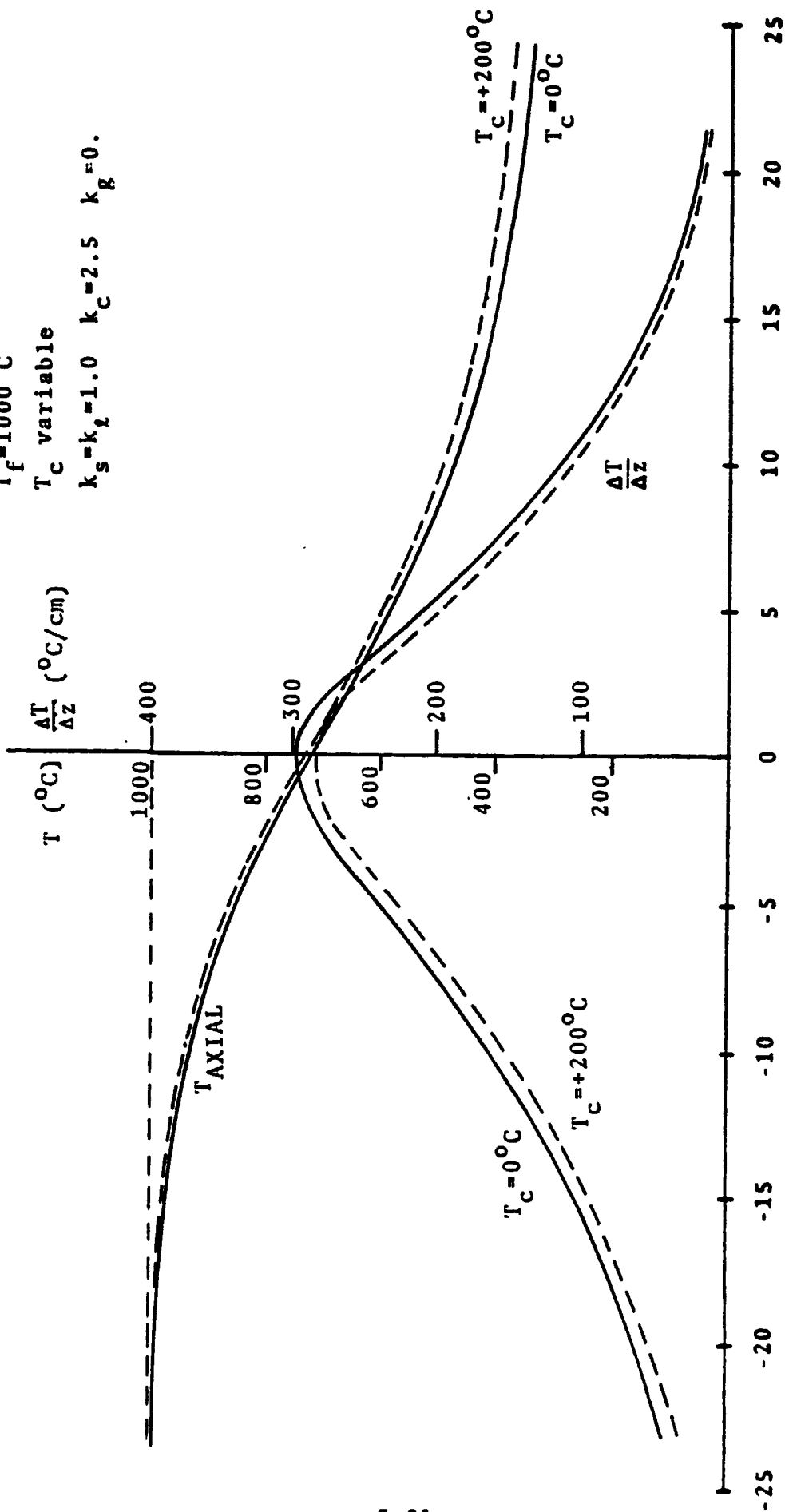
Figure 3-11 presents the axial temperature and thermal gradient for the constant temperature case for the specified range of extractor temperatures. As the plot indicates, less than a 5% ($-12^{\circ}\text{C}/\text{cm}$) increase in maximum thermal gradient is achieved by dropping the extractor temperature from 200°C to 0°C . Table 3.2 provides the achievable gradients for both hot-end temperature configurations over a wide range of extractor temperatures -- including higher extractor temperatures possibly associated with crystal growth in solid solutions of other materials. The table indicates virtually no payoff in requiring an extractor or cooler

Constant Surface Temperature

$T_f = 1000^\circ\text{C}$

T_c variable

$k_s = k_l = 1.0$ $k_c = 2.5$ $k_g = 0$.



Distance from Solid/Liquid Interface (millimeters)

Figure 3-11 Extractor Temperature Effects on the Thermal Profiles for the Constant Hot-End Surface Temperature Configuration

TABLE 3.2 EFFECTIVENESS OF RADIATION COOLING

EXTRACTOR TEMPERATURE	MAXIMUM AXIAL GRADIENT NO BOOST ($T_h = 1000^\circ\text{C}$)	MAXIMUM AXIAL GRADIENT WITH BOOST ($T_h = 1300^\circ\text{C MAX}$)
-270°C	306°C/cm	340°C/cm
-200°C	304°C/cm	336°C/cm
-100°C	303°C/cm	320°C/cm
0°C	300°C/cm	315°C/cm
100°C	295°C/cm	311°C/cm
200°C	288°C/cm	298°C/cm
400°C	252°C/cm	258°C/cm
600°C	180°C/cm	186°C/cm

to produce temperatures less than room temperature (25°C), with very little loss for extractor temperatures considerably warmer.

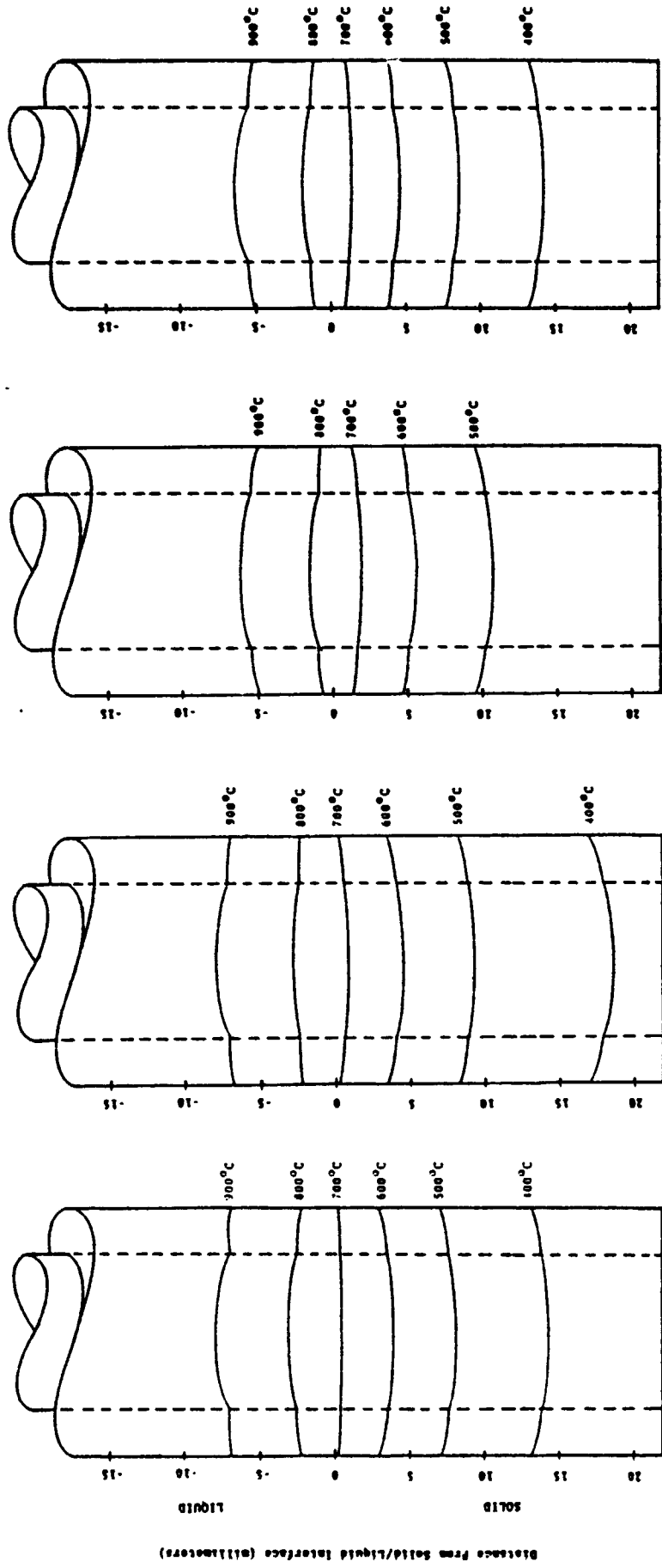
Figure 3-12 presents several isotherm plots to compare the effects of radiative cooling for the two hot-end configurations. The shift in isotherms within each configuration is minor for the corresponding extractor temperatures. A larger temperature movement is introduced by the previously-discussed temperature boost for these extractor temperatures.

3.6 EFFECT OF AMPOULE DIMENSION VARIATIONS

This analysis addressed the effect of ampoule thickness on the thermal profiles within the sample. For this study, the critical temperature boost ($T_{\text{MAX}} = -1250^{\circ}\text{C}$) was assumed on the hot end, and a constant extractor temperature (0° , 200°C) was selected. The baseline sample radius of 5 mm was varied between 2 and 6 mm, with the crucible thickness adjusted accordingly to maintain a thickness-to-sample radius ($\Delta\text{C}/\text{R}$) ratio of 0.6. Additionally, an ampoule configuration consisting of a 6-mm sample radius and a 2-mm crucible thickness ($\Delta\text{C}/\text{R} = 0.333$) was also analyzed.

The axial temperature profiles for the 0°C extractor case are shown in Figure 3-13 for the minimum and maximum radii considered. For the smaller samples (and thinner crucibles), the temperatures are naturally higher in the hot end and cooler in the extractor. Accordingly, a higher thermal gradient at the interface exists for the smaller diameter samples. Figure 3-14 illustrates this trend. The same input temperature profile produces a thermal gradient for a 4-mm diameter sample that is

$k_s = k_l = 1.0$ $k_c = 2.5$ $k_g = 0$.



a) $T_h = 1000^\circ\text{C}$
 $T_c = -270^\circ\text{C}$

$T_h = 1000^\circ\text{C}$
 $T_c = 200^\circ\text{C}$

c) $T_B = 1200^\circ\text{C}$
 $T_C = 200^\circ\text{C}$

d) $T_B = 1250^\circ\text{C}$
 $T_C = -270^\circ\text{C}$

Minimum Boost Temperature

Constant Surface Temperature

Figure 3-12 Radiation Cooling Effects on the Ampoule Isotherms

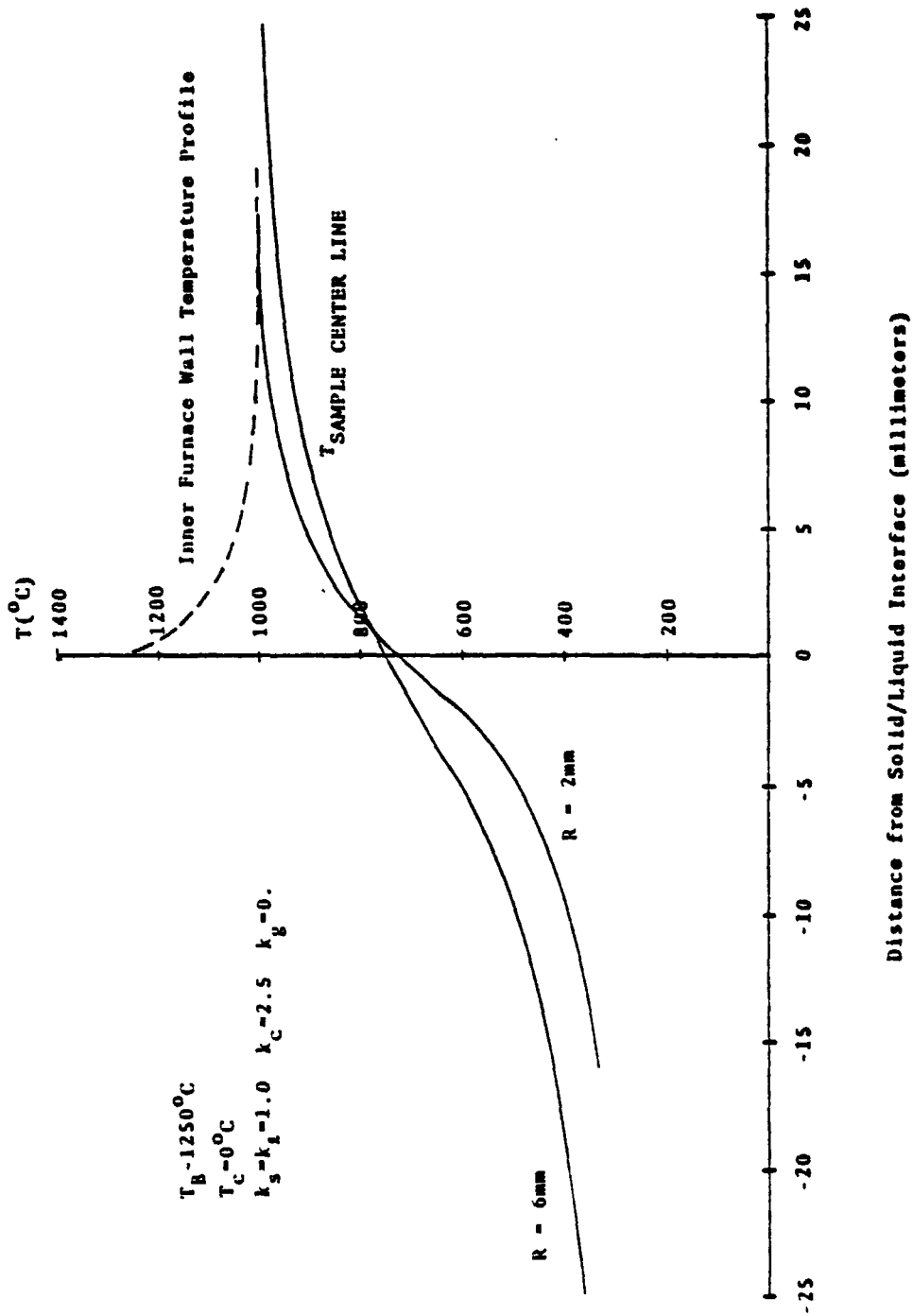
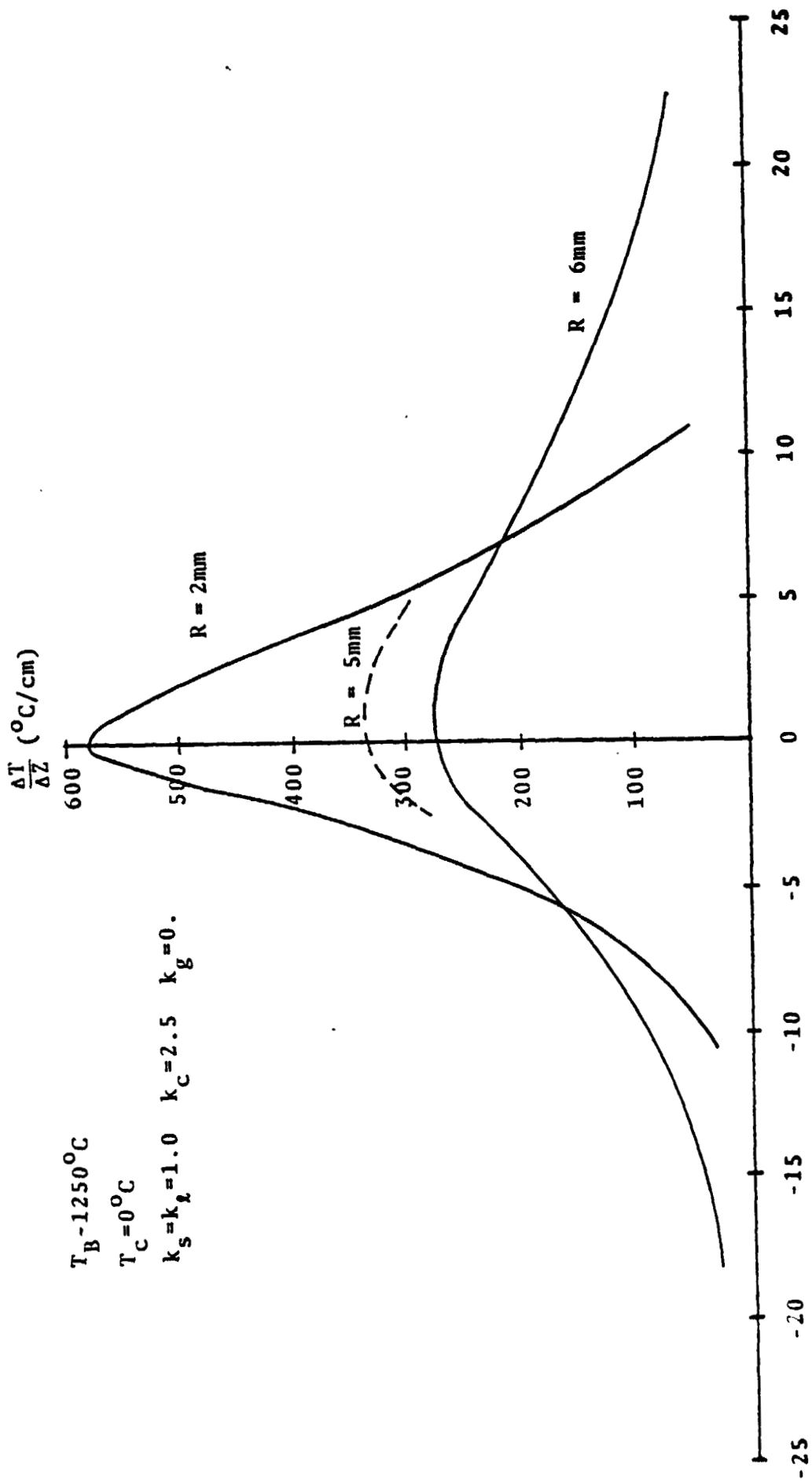


Figure 3-13 Effects of Sample Radius on the Ampoule Centerline Temperature Profile



Distance from Solid/Liquid Interface (millimeters)

Figure 3-14 Axial Thermal Gradient Trend for Variations in Sample Radius

over twice that incurred within a 12 mm diameter sample. Table 3.3 presents the maximum thermal gradient for radii between 2 and 6 mm, for extractor temperatures of 0°C and 200°C. An inverse relationship between radius and thermal gradient would be consistent with the approximation developed for the special case of Section 3.1, i.e.,

$$\frac{\partial T}{\partial z} \leq \frac{8}{3} \left[\frac{T_h - T_m}{d} \right].$$

Further, Figure 3-15 illustrates that the $\partial T/\partial z$ - vs - $1/R$ relationship is nearly linear for the range of radii considered. As the curve indicates, $\partial T/\partial z$ increases at a less than constant rate by decreasing the sample radius, even though the crucible wall thickness and furnace diameter are kept proportional to R .

Figure 3-16 presents a comparison of the isotherms for the $R=2$ mm and $R=6$ mm cases. The higher axial gradients associated with the smaller sample radius are again evident by the "compressed" isotherms, i.e., a greater change in temperature over the same axial distance. Hence, for $R=2$ mm, the hot-end temperatures are hotter and the cool-end temperatures cooler, as previously indicated in Figure 3-13.

Analysis thus far has assumed a constant crucible thickness-to-sample radius ratio ($\Delta C/R$) of 0.6. If this ratio were decreased within the same overall system geometry (e.g., a 6-mm radius ingot in a crucible 2 mm thick), an increase in thermal gradient is realized (Figure 3-17). This improved gradient must be carefully weighed against the possibility of crucible rupture at these high temperatures introduced by the thinner container.

TABLE 3.5 EFFECTS OF CHANGE IN SAMPLE DIAMETER

TEMPERATURE-BOOSTED HOT END				
FURNACE TEMPERATURE		SAMPLE RADIUS R, mm	MAXIMUM THERMAL GRADIENT ($\Delta T/\Delta Z$)	
HOT END (T_B)	COOL END (T_C)			
-1250°C	0°C	6	280°C/cm	
		5	315°C/cm	
		4	385°C/cm	
		3	455°C/cm	
		2	585°C/cm	
-1200°C	200°C	6	270°C/cm	
		5	300°C/cm	
		4	350°C/cm	
		3	425°C/cm	
		2	535°C/cm	

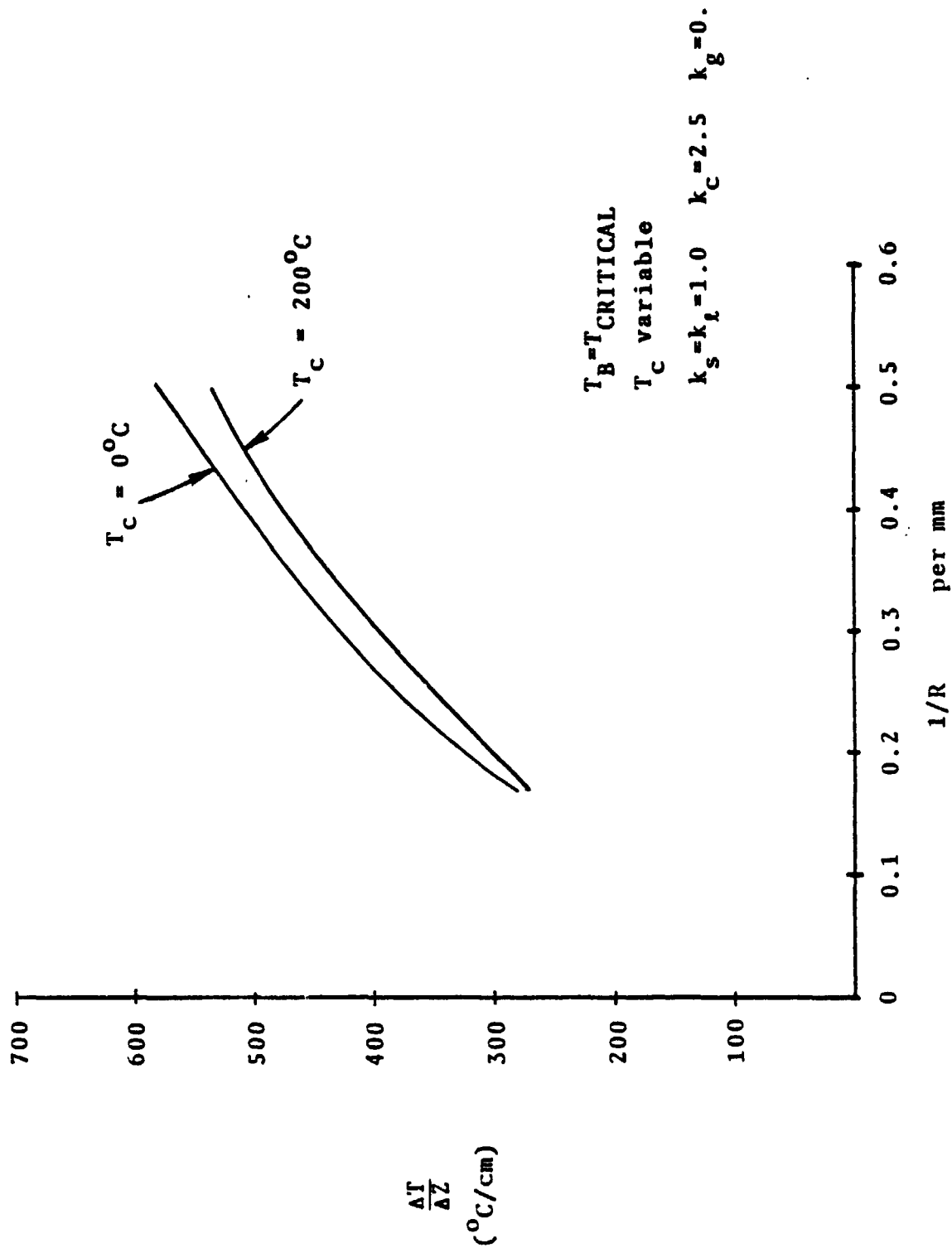
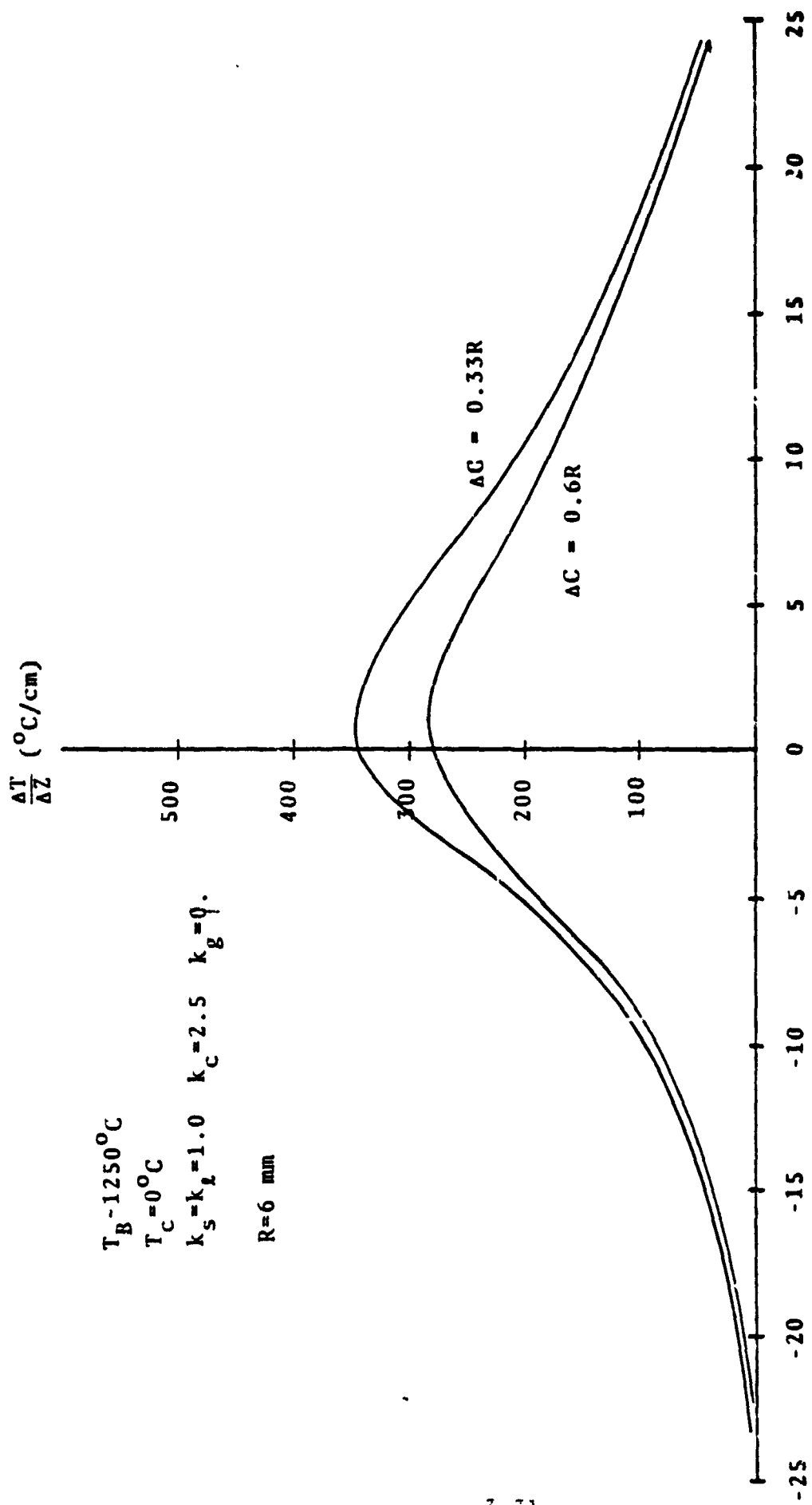


Figure 3-15 Thermal Gradient - versus - Sample Radius Relationship



Distance from Solid/Liquid Interface (millimeters)

Figure 3-17 Effect of Changing Crucible Thickness-to-Sample Radius Ratio

Figure 3-16 compares the isotherms within the two 6-mm radius samples. The higher thermal gradients inherent in the thinner crucible case are again evident around the interface (Figure 3-16c).

3.7 THERMAL CONDUCTION EFFECTS

The thermal conduction characteristics of the various materials composing the Bridgman-Stockbarger configuration play an important role in the heat transfer process required for crystal growth.

As discussed previously, relatively little direct measurement data for thermal conductivities of HgCdTe alloy systems is available. Because of this uncertainty, it is worthwhile to parametrically investigate the thermal profiles within the samples as a function of the assumed thermal conductivity of both the solid and the melt in the HgCdTe system. From the considerations presented in Appendix A, we have adopted nominal values for the thermal conductivity of HgCdTe of 0.5 watt/meter degree and 0.8 watt/meter degree in the melt and solid, respectively.

The conduction characteristics of fused silica are more precisely known (see Appendix A.2.1); however, conductivity of quartz is significantly influenced by impurities in the fused silica, as well by its temperature history. To investigate the implications of these effects, we have varied the crucible conductivity between 1.0 and 2.5 watts/meter-degree to assess the sensitivity of the sample thermal profiles to this conduction medium.

The thermal coupling agent between the crucible and the furnace wall is extremely instrumental in achieving the required

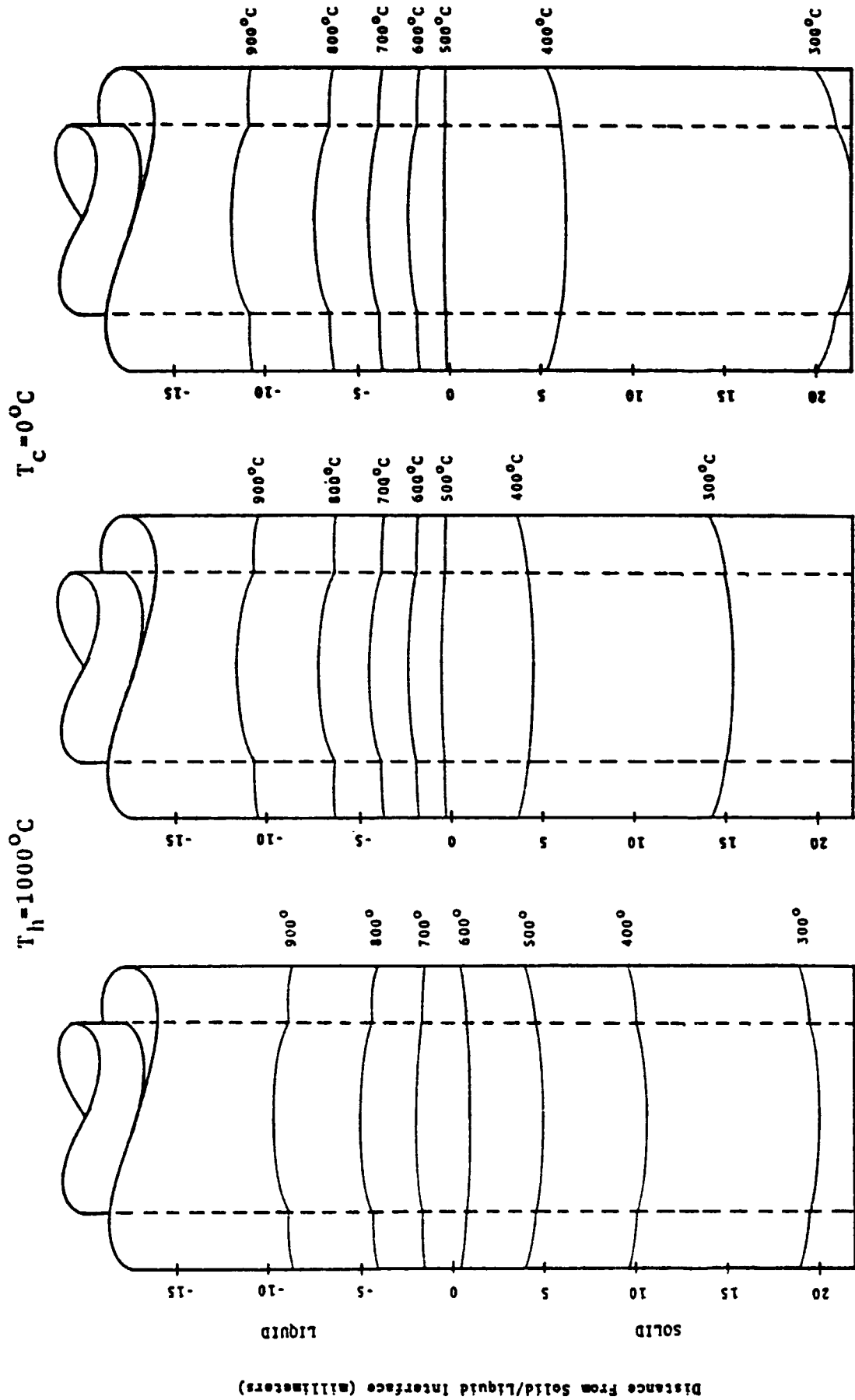
thermal gradients for growth of HgCdTe crystals. This is particularly true in light of the relative insensitivity of the sample thermal condition to radiation cooling and the inability to attain high gradients via this method. Various gasses are available for use as this coupling agent, having thermal conductivities varying from 0.06 watt/meter degree (dry nitrogen) to 0.36 watt/meter degree (helium). For this analysis, we have considered a range of conductivities from 0 (vacuum) to 0.5 watt/meter degree.

One final configuration was also investigated -- the consideration of liquid metal (specifically, gallium) as a heat transfer agent at the cold end of the system. The introduction of this cool-end bath produces a thermal conduction capacity of ~34 watts/meter degree -- a much better heat transport capability than radiative cooling.

Table 3.4 summarizes the effects of the system thermal conductivities on the thermal gradient along the sample centerline. An increase in this gradient is generally produced by higher solid or gas conductivities, and by lower melt or quartz conductivities. The isotherms of Figure 3-18 support these observations. For example, a lower melt conductivity inhibits rapid heat transport toward the interface, which effectively compresses the sample isotherms and increases the gradient in the hot end (compare Figure 3-18a and 3-18b). Similarly, if the solid thermal conductivity is increased, the solid-end heat gradient decreases (see Figure 3-18c), which causes a gradient build-up on the liquid side of the interface. Figures 3-18(d) and (e) indicate the isotherm movements for decreased quartz conductivity and increased

TABLE 3.4 EFFECTS OF THERMAL CONDUCTION

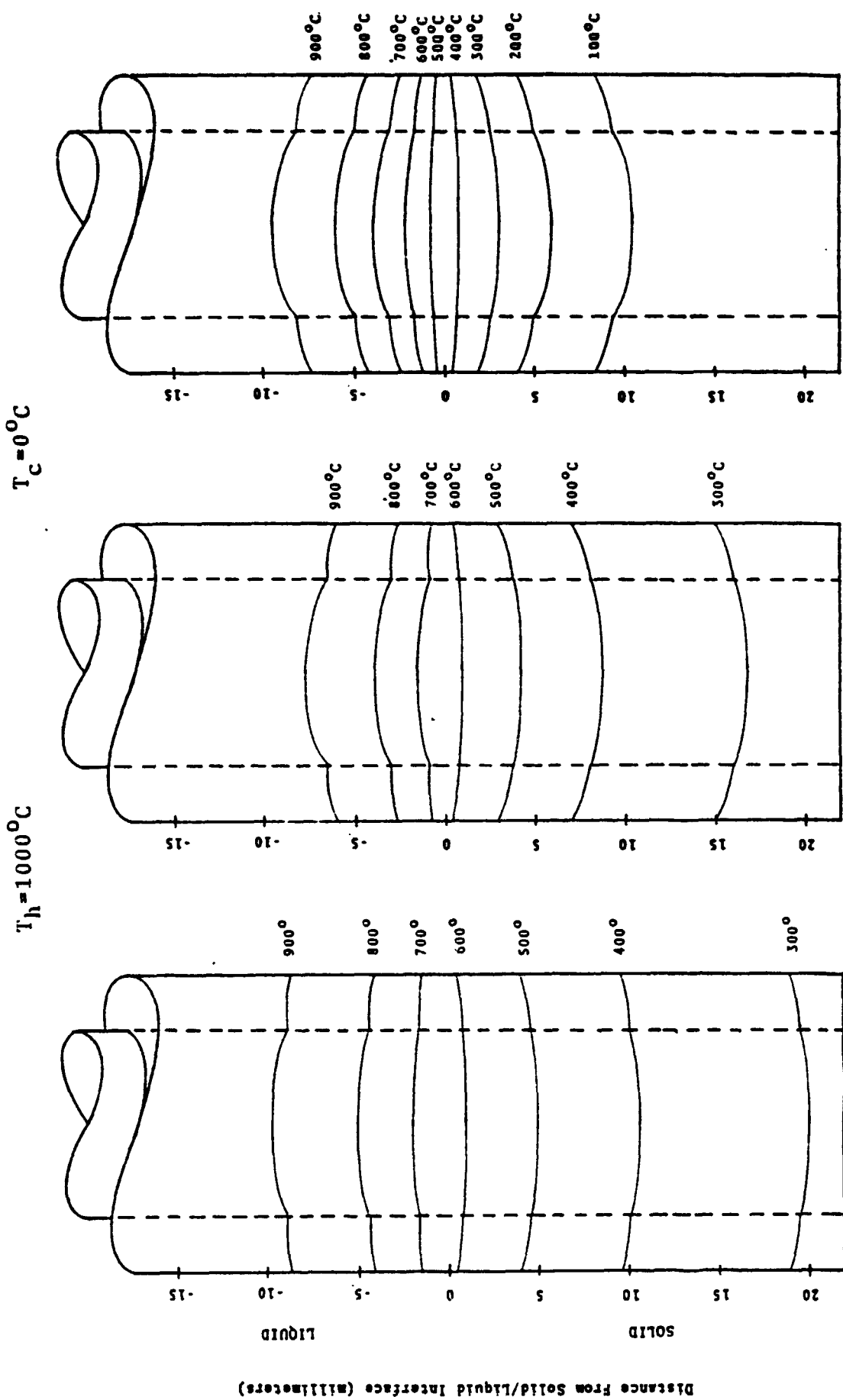
CASE		MAXIMUM GRADIENT (G)	EFFECT
• BASELINE ($k_c=2.5, k_s=0.8,$ $k_l=0.5, k_g=0$)		400°C/cm	
• VARYING CRUCIBLE CONDUCTIVITY, k_c	k_c		Decreasing k_c results in increasing G
	2.2	415°C/cm	
	1.9	425°C/cm	
	1.6	445°C/cm	
	1.3	475°C/cm	
	1.0	500°C/cm	
• VARYING SOLID CONDUCTIVITY, k_s	k_s		Increasing k_s results in increasing G
	2.0	540°C/cm	
	1.6	515°C/cm	
	1.2	475°C/cm	
	0.8	400°C/cm	
	0.6	370°C/cm	
• VARYING MELT CONDUCTIVITY, k_l	k_l		Decreasing k_l results in increasing G
	0.6	380°C/cm	
	0.45	425°C/cm	
	0.4	445°C/cm	
	0.3	505°C/cm	
	0.2	580°C/cm	
• VARYING GAS CONDUCTIVITY, k_g	k_g		Increasing k_g results in increasing G
	0.1	545°C/cm	
	0.2	620°C/cm	
	0.3	675°C/cm	
	0.4	715°C/cm	
	0.5	740°C/cm	



a) BASELINE b) LOW MELT CONDUCTIVITY c) HIGH SOLID CONDUCTIVITY

$k_S = 0.8$ $k_L = 0.5$ $k_C = 2.5$ $k_g = 0$ $k_S = 2.0$ $k_L = 0.2$

Figure 3-18 Thermal Conduction Effects on the Ampoule Isotherms



a) BASELINE $k_s = 0.8$ $k_l = 0.5$ $k_c = 2.5$ $k_g = 0$

d) LOW QUARTZ CONDUCTIVITY $k_c = 1.0$

e) HIGH GAS CONDUCTIVITY $k_g = 0.5$

Figure 3-18 Thermal Conduction Effects on the Ampoule Isotherms (Continued)

gas conductivity, respectively. Figure 3-18(e) particularly illustrates the compressed isotherms (i.e., high gradients) associated with increased thermal conduction through the coupling agent between the crucible and the furnace wall.

As a means of increasing the thermal gradient, a liquid gallium bath at one or both ends presents an attractive option. Since gallium has a low melting point (29°C), a low vapor pressure, and a good thermal conductivity (34 watt/meter-degree at 60°C), it is compatible for use in an evacuated system and is easy to work with. Figure 3-19 presents axial temperature and thermal gradient profiles, and Figure 3-20 the isotherms for the case of a gallium bath used for cooling and vacuum at the hot end of the furnace. A gradient of 650°C is achieved, though this is not at the desired 700°C point. Appropriate temperature adjustments could correct this with a small loss in gradient.

As Figure 3-18(a) indicates, the critical 700° (crystallization) isotherm for HgCdTe has been displaced by almost 2 mm from the mid-plane position of the B-S configuration for the $T_h=1000^{\circ}\text{C}$, $T_c=0^{\circ}\text{C}$ configuration. To drive the isotherms back toward this mid-plane position, the extractor temperatures must be raised accordingly. Figure 3-21 illustrates the desired isotherm conditions for both the constant surface temperature and the temperature boost configurations. The required extractor temperatures for these cases are 400°C and 330°C , respectively. The corresponding achievable gradients are $325^{\circ}\text{C}/\text{cm}$ and $360^{\circ}\text{C}/\text{cm}$ -- indicating an ~10% increase in thermal gradient with the boosted temperature configuration.

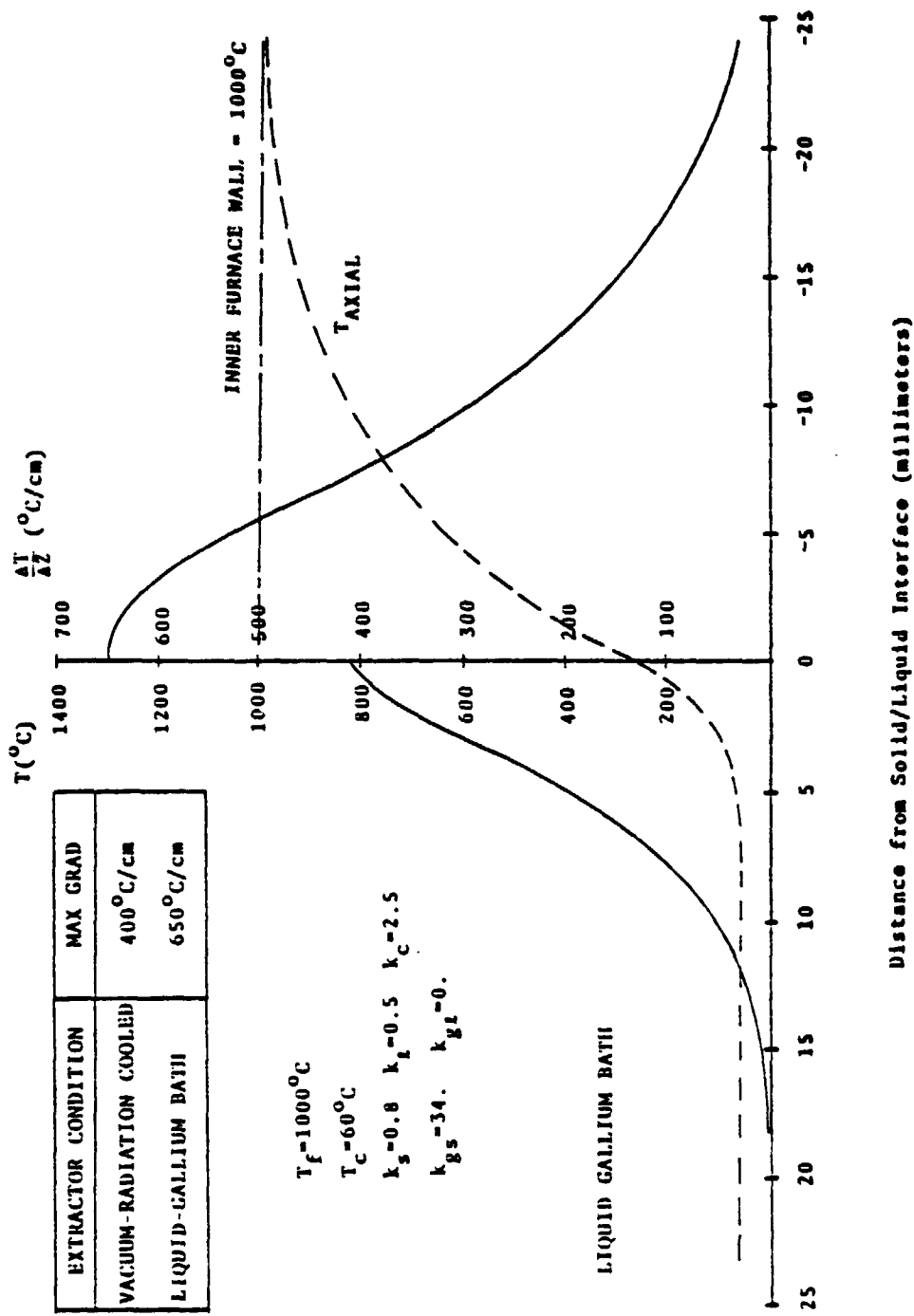
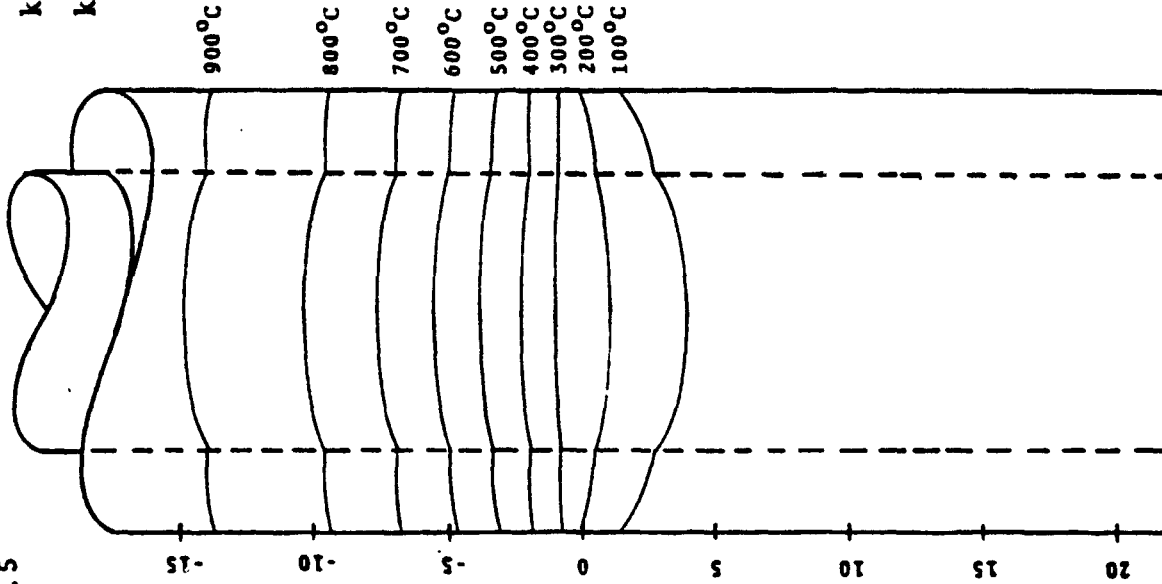


Figure 3-19 Thermal Profiles for the Liquid Gallium Bath Growth Configuration (Cool End)

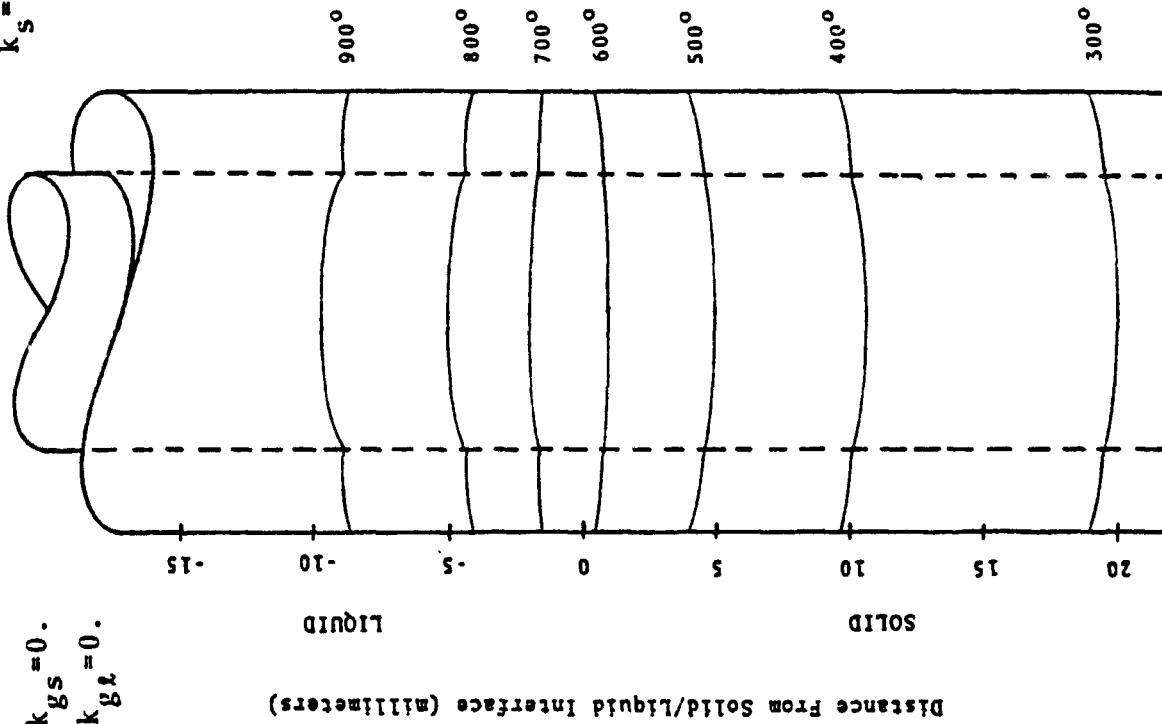
$T_h = 1000^\circ\text{C}$ $T_c = 60^\circ\text{C}$

$k_{gs} = 34$
 $k_{gl} = 0$



b) LIQUID GALLIUM BATH

$k_s = 0.8$ $k_l = 0.5$
 $k_c = 2.5$



a) RADIATION-COOLED/VACUUM

Figure 3-20 Effects of the Liquid Gallium Bath on the System Isotherms

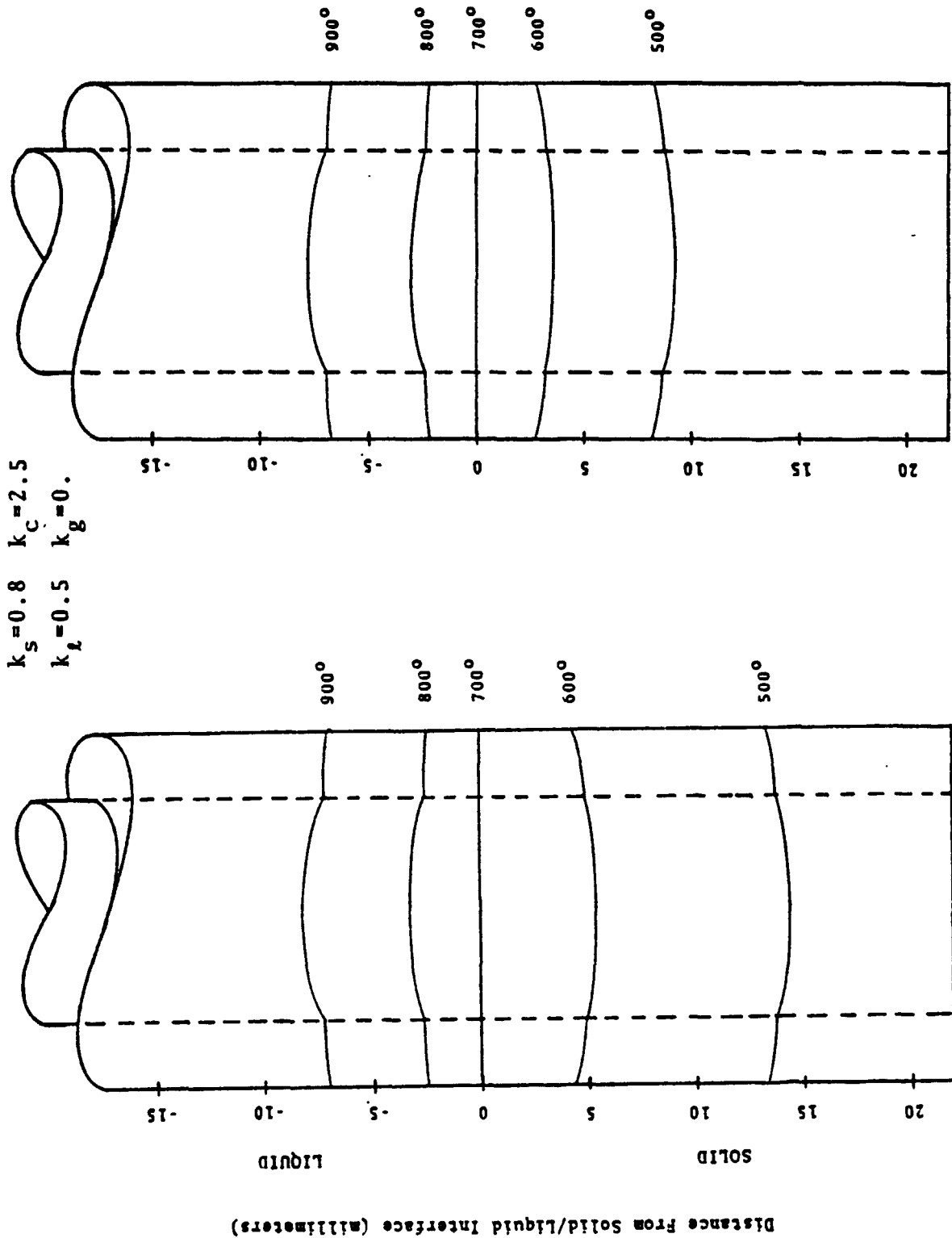
$T_h = 1000^\circ\text{C}$ $T_c = 0^\circ\text{C}$

$k_{gs} = 0$
 $k_{gl} = 0$

Distance From Solid/Liquid Interface (millimeters)

LIQUID

SOLID



a) Constant Surface Temperature $T_h = 1000^\circ\text{C}$ $T_c = 400^\circ\text{C}$
 b) Temperature Boost $T_B = -1200^\circ\text{C}$ $T_C = 330^\circ\text{C}$

Figure 3-21. Bridgman-Stockbarger Configurations Producing the Required 700°C Isotherm at the Mid-Plane Position.

3.8 EFFECT OF GROWTH VELOCITY

The steady state differential equation for the temperature T within the ampoule includes a heat transport term $\beta \frac{\partial T}{\partial z}$, where β is the growth rate v divided by the thermal diffusivity of the material. As indicated in Appendix A, we can express the diffusivity as

$$\text{Diffusivity}_i = 8.17 \times 10^{-7} k_i \text{ meter}^2/\text{sec}$$

where k_i is the thermal conductivity of medium i , if we use the Dulong and Petit specific heat and a density of 7600 kg/m^3 .

For all analyses presented thus far, we have assumed no growth rate, i.e., $v = \beta = 0$. In this analysis, we now parametrically consider growth rates from one millimeter per hour to one meter per hour to investigate the effects of ampoule movement. The growth configuration considered was the constant temperature furnace wall, with $T_h = 1000^\circ\text{C}$, $T_c = 0^\circ\text{C}$.

Figure 3-22 illustrates the trends of the axial thermal gradient for the range of growth velocity considered. Table 3.5 summarizes the maximum gradients achieved for this range of growth velocities. Note that growth rates below -5 cm/hr have little, if any, appreciable effect on the maximum gradient near the interface. Less than 5% improvement in effectiveness is realized with even faster growth rates, until such time that the growth rate becomes large enough that the isotherms are swept almost completely into the solid end and the gradients begin to decrease (Figure 3-23).

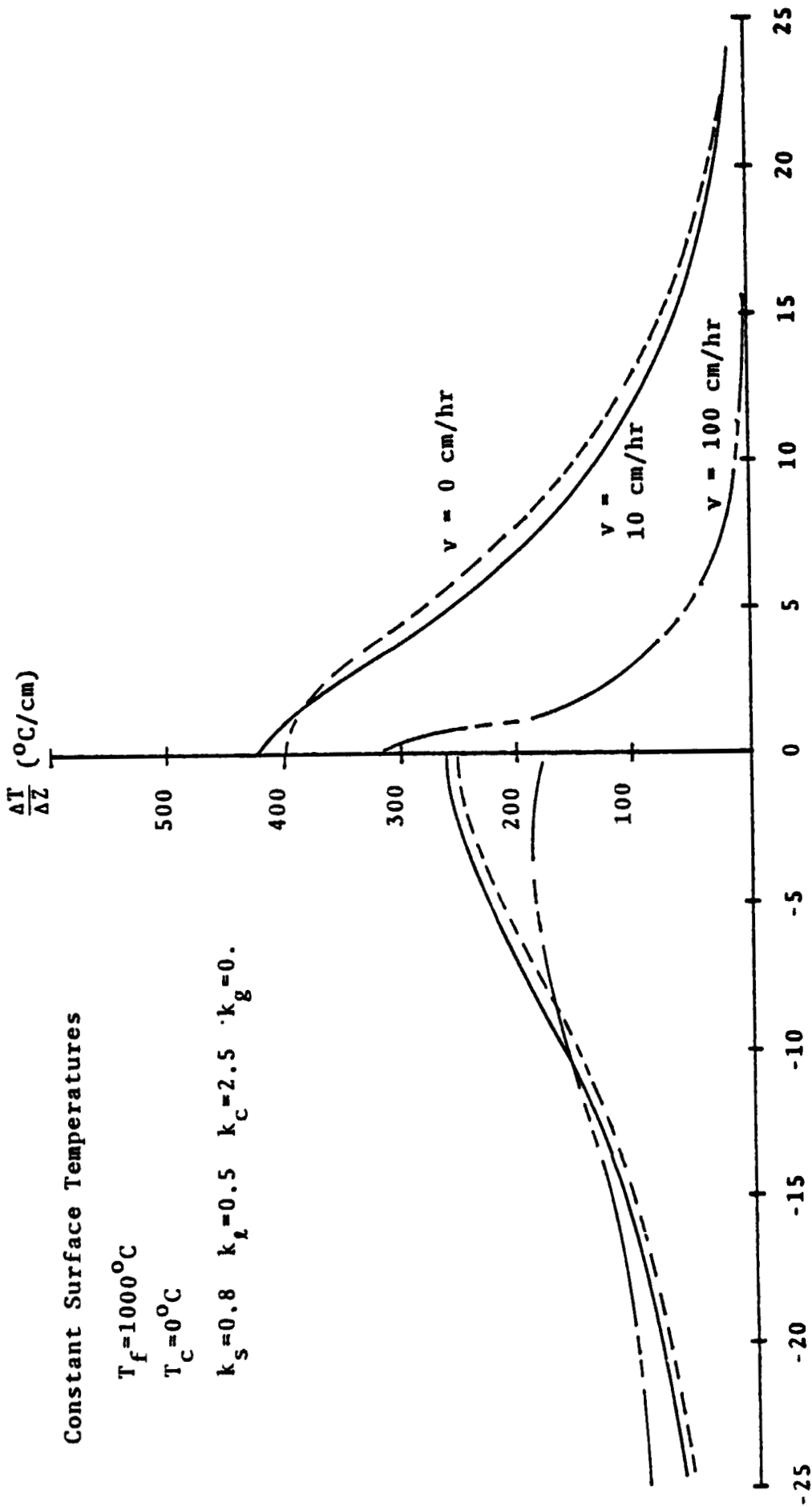


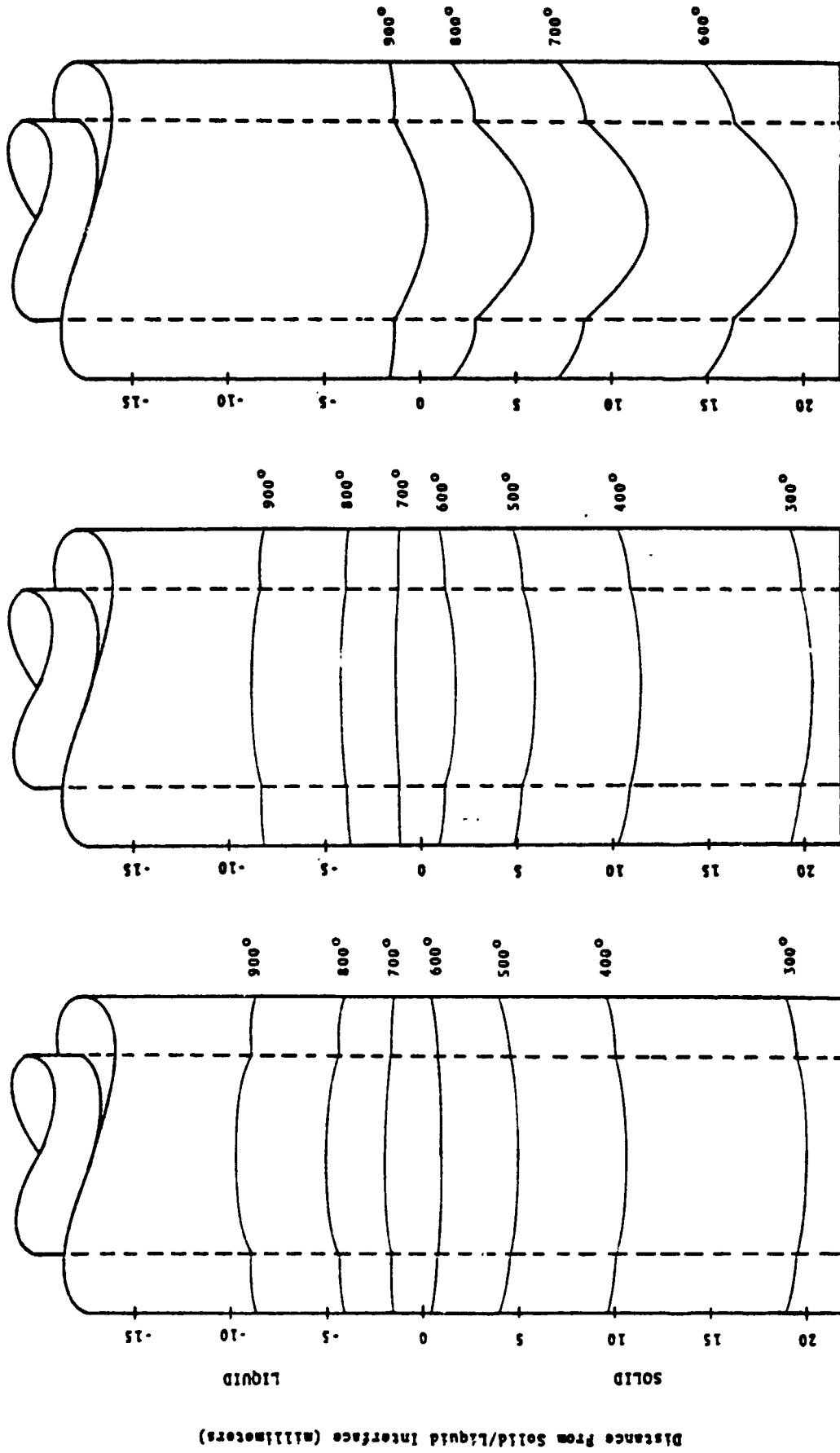
Figure 3-22 Effects of Growth Velocity on the Axial Thermal Gradient

TABLE 3.5 EFFECT OF GROWTH VELOCITY
ON THERMAL GRADIENT

GROWTH VELOCITY, v (cm/hr)	MAXIMUM THERMAL GRADIENT (°C/cm)
0	400
0.36	405
1.08	407
3.6	415
10.8	425
36.0	420
100.8	320

$T_h = 1000^\circ\text{C}$
 $T_c = 0^\circ\text{C}$

$k_s = 0.8$ $k_l = 0.5$
 $k_c = 2.5$ $k_g = 0$



a) $v=0$
 (No Growth Velocity)

b) $v=10$ cm/hr

c) $v=100$ cm/hr

Figure 3-23 Isotherm Movement as a Function of Growth Rate

4.0 REFERENCES

1. Steininger, J., *Journal of Electronic Materials*, Volume V, pp. 229-321, 1976.
2. Takase, Y., *Japan Journal of Applied Physics*, Volume XIII, pp. 539-540, 1974.
3. Tiller, W. A., K. A. Jackson, J. W. Rutter, B. Chalmers, *Acta Metallurgica*, Volume I, p. 428, 1953.
4. Long and Schmit, "Mercury-Cadmium Telluride and Closely Related Alloys," Chapter 5 of Volume V, *Semiconductors and Semimetals*.
5. Zanio, "Cadmium Telluride," Volume XIII, p. 112, *Semiconductors and Semimetals*.
6. Touloukian, Y. S., Thermal/Physical Properties Research Center (TPRC), *Thermal/Physical Properties of High Temperature Solid Material*, Volume I, p. 1407, Figure 419, McMillan, New York, 1967.
7. *Ibid.*, Volume VIII, p. 1239, Figure 462.
8. Blair and Newnham, *Preparation and Physical Properties of Crystals in the HgTe-CdTe Solid Solution Series and Metallurgy of Elemental and Compound Semiconductors*, Interscience, New York, 1961.
9. Kuigery, Bowen and Uhlman, *Introduction to Ceramics*, Second Edition, p. 626, Wiley, New York.
10. Carslaw, H. S., J. C. Jaeger, *Conduction of Heat in Solids*, Second Edition, Oxford University Press, 1959.

PRECEDING PAGE BLANK NOT FILMED

APPENDIX A

SYSTEM THERMAL PROPERTIES

A.1 PROPERTIES OF HgCdTe

A.1.1 Thermal Conductivity

Very little reliable work has been done in the direct measurement of the thermal conductivity of HgCdTe alloys, and so we are forced to rely on extrapolation and interpolation to a great degree. We do have some data for CdTe and for HgTe which are helpful.

Long and Schmit⁴ report that at 77°K CdTe has a thermal conductivity of 40 watts/meter-degree, and that k varies with $T^{-1.3}$ at least to 300°K. Also that HgTe at 77°K has $k = 15$ watts/meter-degree, and that k varies with T^{-1} to 300°K. Furthermore, they report "a shallow minimum" in the alloys for a composition of $\text{Hg}_{0.8}\text{Cd}_{0.2}\text{Te}$, which happens to be close to the composition of particular interest.

Zanio⁵ shows a curve for the thermal conductivity of CdTe which indicates that the T^{-1} law is probably valid to and beyond 1000°K.

The TPRC data series⁶ gives plots for the thermal conductivity of $\text{Hg}_{.96}\text{Cd}_{.04}\text{Te}$ and $\text{Hg}_{.93}\text{Cd}_{.07}\text{Te}$ up to 300°K.

Polycrystalline material is expected to have a lower thermal conductivity than monocrystal, but this effect should not be important at high temperature.

From the above considerations we have adopted single best values for the thermal conductivity of HgCdTe in the melt and

in the solid of 0.5 watt/meter-degree and 0.8 watt/meter-degree respectively, and we have tested values varying above and below. We have performed specific analyses using equal values in the solid and liquid phases where it was important to show the effects of varying other parameters without the interference of a step change in conductivity.

A.1.2 Emissivity

The emissivity data for HgCdTe is also far from copious, and the use of sharply defined values would be dubious in this work in any event as much depends on the surface condition of the sample and on the nature of the crucible (fused silica) interface. It is known, for example, that as solid HgCdTe cools it shrinks back from the crucible wall, and that at the instant of separation the effective total emissivity drops sharply.

Based on TPRC ⁷ data for CdTe for the hemispherical infrared spectral emittance, we have chosen 0.3 as the baseline value for the total emittance in both solid and liquid. This value is higher than the value typical of materials such as germanium, but it is justified.

A.1.3 Thermal Diffusivity

The thermal diffusivity is calculated from the equation

$$\text{diff} = k/\rho C$$

where k = thermal conductivity

o = density

C = specific heat

The thermal conductivity is discussed above.

We have excellent data on the mass density of $\text{Hg}_{1-x}\text{Cd}_x\text{Te}$, e.g., Blair and Newnham⁶, who give the data for the following table:

x	ρ (g/cm ³)
0	8.07
0.05	7.91
0.1	7.84
0.2	7.62
0.4	7.17
1.0	5.81

It was judged unproductive to make an exhaustive study of the specific heat, as the thermal conductivity is so poorly known. Thus we have simply used the Dulong and Petit law that the specific heat per mole is $3R$. We use the classical value rather than the Debye law as we are working near the melting point, well above the Debye temperature. Hence, $C = 25$ joules/mole degree. For $\text{Hg}_{0.8}\text{Cd}_{0.2}\text{Te}$, the molecular weight is 0.31058 kg/mole and from the above table the mass density is 7620 kg/meter³. Thus the molar density is 24.6×10^3 mole/meter³. The diffusivity is given by

$$\text{Diffusivity} = \frac{k}{2 \times 24.6 \times 10^3 \times 25} = 8.17 \times 10^{-7} k \frac{\text{m}^2}{\text{sec}}$$

where k is in watts/meter-degree.

A.2 PROPERTIES OF FUSED SILICA

A.2.1 Thermal Conductivity

The thermal conductivity of fused silica glass requires a special treatment for this analysis, as either of the two processes (radiation photon or phonon) may dominate, depending on temperature. Furthermore in a system in which large gradients are present, the phonon and photon fields will be very far from mutual thermal equilibrium, and care must be exercised in the definition of temperature.

Fortunately, for fused silica, it is possible to make conductivity measurements which exclude radiation, and photon mean free paths are either very short or very long compared to the system dimensions, depending on wavelength. Discussion of this can be found in Kuigery, Gowen and Uhlman⁹, and the application is discussed in Appendix B of this report.

Data for the spectral photon transparency of fused silica have been taken from the Awersil bulletin for T-0 commercial grade fused silica and approximations were made as explained in Appendix B (Table B.1 results).

Phonon conduction in single phase glasses increases with temperature only at low temperatures. At high temperatures, the phonon mean free path is limited by the highly disordered network structure to the order of interatomic distances. Thus above about 800°K the phonon conductivity is nearly constant, with slightly higher values for pure silica than for the more complex borosilicate or soda-lime glasses. Conductivity is significantly influenced by impurities in fused silica, as well

as by its thermal history.

We have taken the fixed value $k_c = 2.5$ watts/meter-degree as our phonon conductivity baseline value, and have varied this for effect in the parametric analysis.

A.3 PROPERTIES OF THE THERMAL COUPLING AGENT BETWEEN THE CRUCIBLE AND THE FURNACE WALL

A.3.1 Thermal Conductivity

Three cases were considered. The coupling agent may be a vacuum allowing only pure radiative transfer, it may be a gas allowing both radiation and conduction (convection is not allowed) or it may be a liquid metal such as gallium.

The various possible gasses have widely varying thermal conductivities. For example, helium at 1000°K has a conductivity of 0.36 watt/meter-degree, while dry nitrogen at 1000°K has a conductivity of only 0.063 watt/meter-degree. Thus within limits the gas conductivity may be considered an experimenter controlled parameter. The CRC Handbook gives useful tables for gas conductivity.

Liquid metal was considered as a heat transfer agent only at the cold end of the system, and for this purpose gallium was chosen as an example. The thermal conductivity of gallium at 60°C is 34 watts/meter-degree, while the melting point is slightly below 30°C .

PRECEDING PAGE BLANK NOT FILMED

APPENDIX B

NUMERICAL SOLUTION TO THE THERMAL PROBLEM

In formulating the thermal problem for the Bridgman-Stockbarger configuration, we did not initially specify the characteristics of the furnace system. Rather, we specified the thermal conditions required within the material sample, together with the thermal characteristics and constraints of the B-S system. This specified environment defines the boundary conditions and physical constants for the problem under analysis. If a unique thermal profile is not dictated by these boundary conditions, then it is possible to optimize some aspects of the problem -- for example, developing a system with minimal power consumption, maximum thermal gradient at the interface, etc. Once the desired thermal conditions for the ampoule have been determined, the ampoule surface temperature, the heat flux, and the coupling effects to the furnace wall imply the furnace specifications.

This effort has been concerned with determining optimum ampoule thermal conditions and the generation of furnace specifications, and did not address the performance of a particular furnace design. Thus, the numerical techniques used to solve this thermal problem were not concerned with furnace design other than the inner wall and the associated thermal coupling to the outer crucible wall.

B.1 THE DIFFERENTIAL EQUATION

In formulating this thermal problem, we have made the

following assumptions:

- There is cylindrical symmetry within the ampoule.
- All time-dependent transients have subsided.
- The solidification rate is sufficiently slow that the latent heat of fusion can be ignored.

This latter assumption can be relaxed if necessary, but the heat of fusion is negligible in most practical systems -- especially those requiring very small mean growth rates (i.e., solid solutions).

The steady state differential equation for the temperature T within the ampoule then is

$$\frac{k}{\rho C_p} \left\{ \frac{\partial^2 T}{\partial r^2} + \frac{1}{r} \left(\frac{\partial T}{\partial r} \right) + \frac{\partial^2 T}{\partial z^2} \right\} - v \frac{\partial T}{\partial z} = 0 \quad (1)$$

where the thermal diffusivity $K/\rho C_p$ is assumed constant for any one phase or material (solid, melt, or silica container). In this equation, k is the thermal conductivity, ρ is density, C is the heat capacity, r and Z are the cylindrical reference coordinates (r is radial position, z is the axial position away from the heater-cooler boundary), and v is the growth rate (i.e., $v \frac{\partial T}{\partial z}$ is a heat transport term).

If we let

$$\phi = \frac{T - T_c}{T_h - T_c},$$

we have normalized the temperature from 0 to 1 as T varies from T_c to T_h , the low and high temperature asymptotes of the system. Since $d\phi/dx = \frac{dT/dx}{T_h - T_c}$ where x is any coordinate, substitution of ϕ for T in equation (1) is immediate so that

$$\frac{\partial^2 \phi}{\partial r^2} + \frac{1}{r} \left(\frac{\partial \phi}{\partial r} \right) + \frac{\partial^2 \phi}{\partial z^2} - \beta \frac{\partial \phi}{\partial z} = 0, \text{ with } \beta = \frac{\rho C v}{k} \quad (2)$$

The above differential equation, which reduces to Laplace's Equation when there is zero growth rate for the system, has been solved using finite difference techniques to perform the Bridgman-Stockbarger thermal analysis.

B.2 FINITE DIFFERENCE EQUATIONS

For the finite difference technique, it is necessary to describe the physical problem by defining a "grid" or node point structure throughout the system of interest, and further to specify the interaction of each node point with its neighboring node points. For the B-S configuration, there are two independent variables -- r and z . For this study, we have defined the region of interest as illustrated in Figure B-1, i.e., $r \geq 0$ from symmetrical considerations and z extending away from the liquid-solid interface in either direction to a distance equal to 5 times the sample diameter ($z > 0$ in the solid, $z < 0$ in the liquid).

This region has been divided into equal divisions such that node points are indicated by the coordinates $r_i = i\delta$ and $z_j = j\delta$ where δ is the dimension of the node cell. The temperature at the ij node then is specified as ϕ_{ij} , that is, the value of ϕ at $r = r_i$ and $z = z_j$. To arrive at the finite difference equation corresponding to (2), the following results¹⁰ are utilized (ignoring higher order terms):

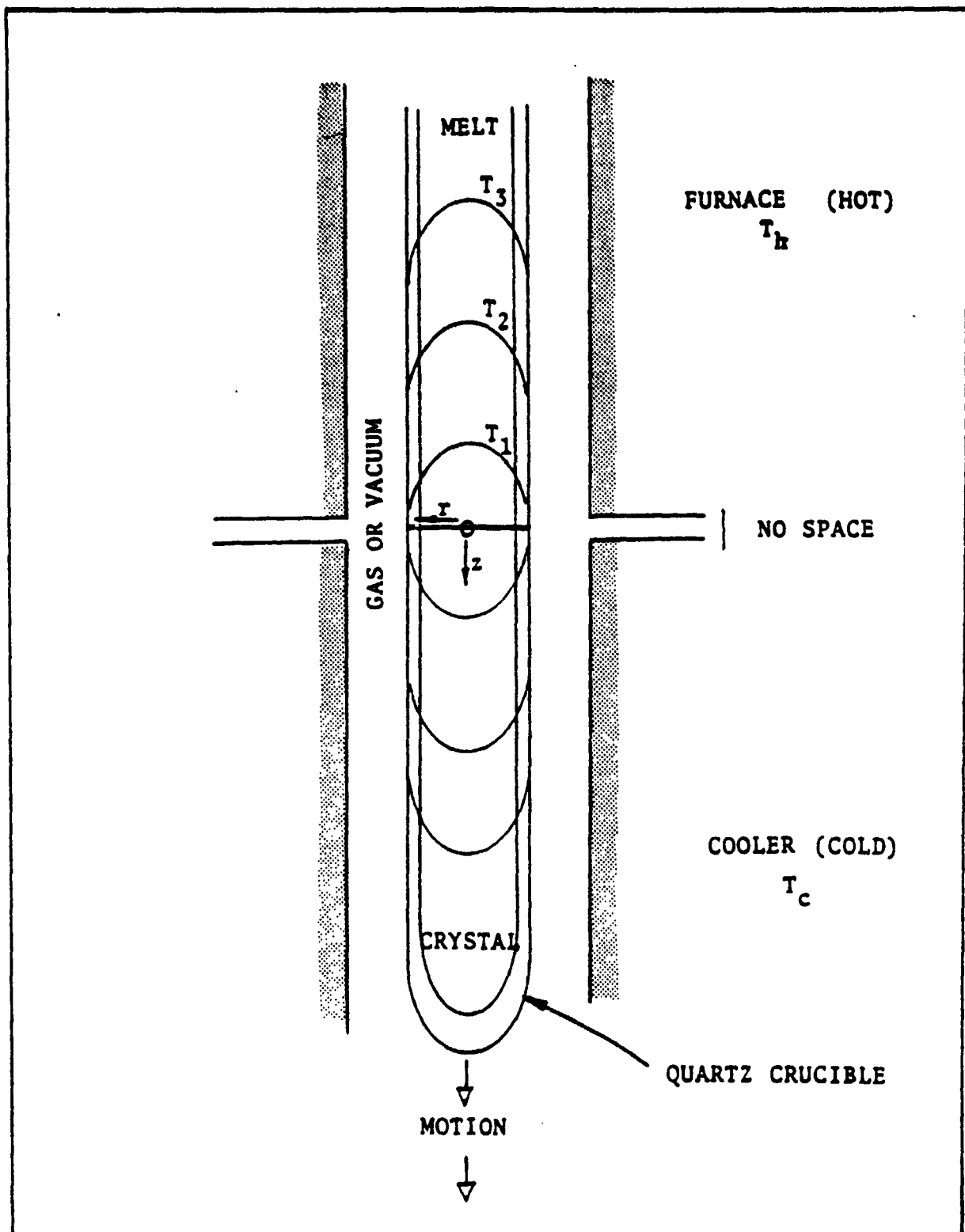


Figure B-1 Bridgman-Stockbarger Growth Environment

$$\left. \frac{df}{dx} \right|_m = (f_{m+1} - f_{m-1})/2\delta$$

$$\left. \frac{d^2f}{dx^2} \right|_m = (f_{m+1} - 2f_m + f_{m-1})/\delta^2$$

For the purposes of this study, it is also desirable to have

$$\left. \frac{d^2f}{dx^2} \right|_m + \frac{1}{x} \left. \frac{df}{dx} \right|_m = \frac{1}{2m\delta^2} \left\{ (2m-1)f_{m-1} - 4mf_m + (2m+1)f_{m+1} \right\} \text{ for } m \neq 0$$

and
$$= \frac{4}{\delta^2} (f_1 - f_0) \text{ for } m=0.$$

Writing these equations for the two variables of interest produces

$$\left. \frac{\partial \phi}{\partial z} \right|_{i,j} = \frac{1}{2\delta} (\phi_{i,j+1} - \phi_{i,j-1}) \quad (3)$$

$$\left. \frac{\partial^2 \phi}{\partial z^2} \right|_{i,j} = \frac{1}{\delta^2} (\phi_{i,j-1} - 2\phi_{i,j} + \phi_{i,j+1}) \quad (4)$$

$$\left. \frac{\partial^2 \phi}{\partial r^2} \right|_{i,j} + \frac{1}{r} \left. \frac{\partial \phi}{\partial r} \right|_{i,j} = \frac{1}{2i\delta^2} \left\{ (2i-1)\phi_{i-1,j} - 4i\phi_{i,j} + (2i+1)\phi_{i+1,j} \right\} \quad (5)$$

Substitution of these equations into (2) and solving for ϕ at the ij node eventually yields

$$\phi_{i,j} = 1/4 \left\{ \left(1 - \frac{1}{2i}\right) \phi_{i-1,j} + \left(1 + \frac{1}{2i}\right) \phi_{i+1,j} + \left(1 - \frac{\delta\beta}{2}\right) \phi_{i,j+1} + \left(1 + \frac{\delta\beta}{2}\right) \phi_{i,j-1} \right\} \quad i \neq 0 \quad (6)$$

and

$$\phi_{0,j} = 2/3 \phi_{1,j} + \left(\frac{2 - \beta\delta}{12}\right) \phi_{0,j+1} + \left(\frac{2 + \beta\delta}{12}\right) \phi_{0,j-1} \quad i = 0 \quad (7)$$

It should be noted that the effects of the cylindrical system have been incorporated into (6) via the radial correction term $1/2i$. This correction indicates that the temperature at a node point is not exactly the mean of the four surrounding node points, but is affected more by the larger-radius temperature because of the "surrounding" nature introduced by the grid curvature effects. This factor becomes less important as the radius increases away from the sample centerline. A similar correction for a moving ampoule (i.e., non-zero growth rate) is also evident in these equations.

Equations (6) and (7), representing solutions for internal node points, can be used together with the appropriate boundary conditions in an iterative fashion to obtain the values of ϕ (hence T) for all system node points. Care must be taken to ensure that the appropriate value of thermal diffusivity corresponding to the material at each node point be incorporated into these equations. Desired thermal gradients can then be obtained from the ϕ_{ij} values within the numerical accuracy of the procedure.

B.3 TREATMENT OF BOUNDARY CONDITIONS

Boundary conditions must be treated differently from the "internal" node points. Figure B-2 diagrams the Bridgman-Stockbarger growth configuration and indicates the types of boundary conditions encountered in this thermal problem.

A fused silica (also called "quartz") ampoule is in a furnace/cooler (also referred to as "extractor") combination. This ampoule contains an ingot, the top part of which is melted, the lower part recrystallized. Heat flow is into the top part of the ampoule, out the bottom. The conditions at the various interfaces (e.g., crystal-melt, melt-crucible, crystal-crucible, crucible-furnace) are set by laws of continuity. These laws are determined by the nature of the particular interface, and may generally be approximated by one (or a combination) of the following boundary conditions:

- Prescribed surface temperature or surface temperature function.

Due to materials limitations (e.g., fused silica rupture strength), it may be meaningful to consider cases where the temperature is prescribed on a system surface such as the sample, crucible, or furnace wall (Figure B.3). While it may not be possible in practice to fix the exact temperature of the melt or crystal surface, nevertheless the differential equation (2) may be integrated directly under these conditions to provide solutions which give valuable insight into the nature of the physical problem.

- Heat conduction across a surface.

In this case, heat flow continuity requires that

$$k_1 \left. \frac{\partial T}{\partial n} \right|_1 = k_2 \left. \frac{\partial T}{\partial n} \right|_2$$

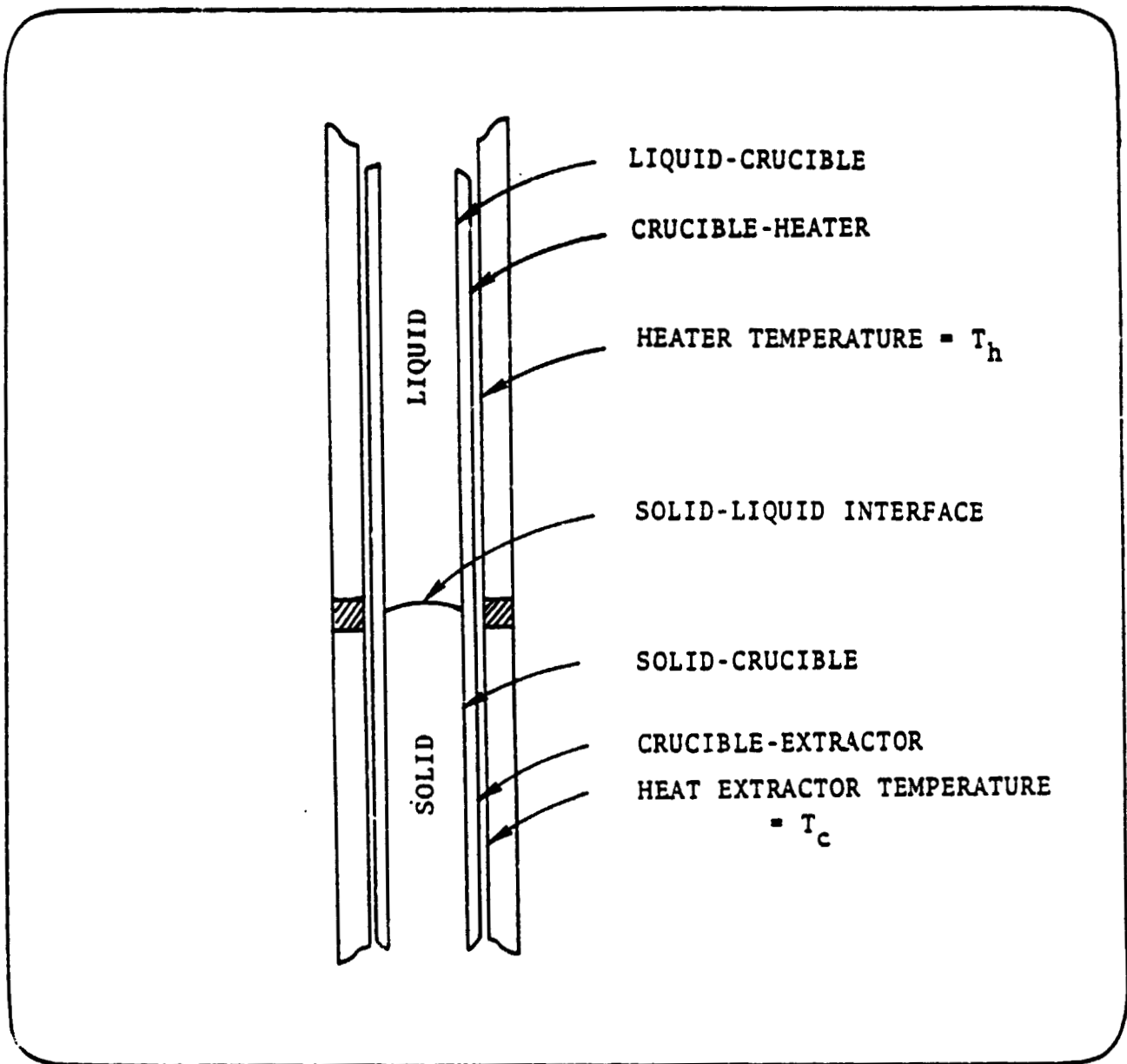


Figure B-2 Boundary Conditions for the Bridgman-Stockbarger System

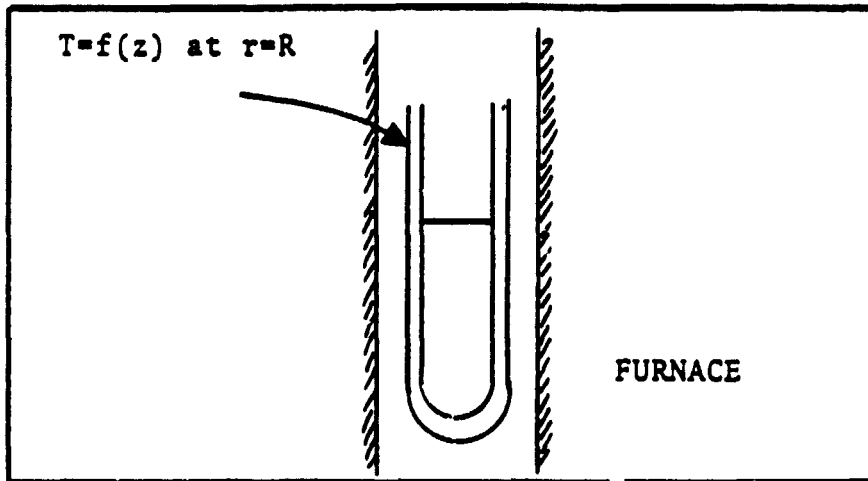


Figure B-3 Prescribed Surface Temperature Boundary Condition

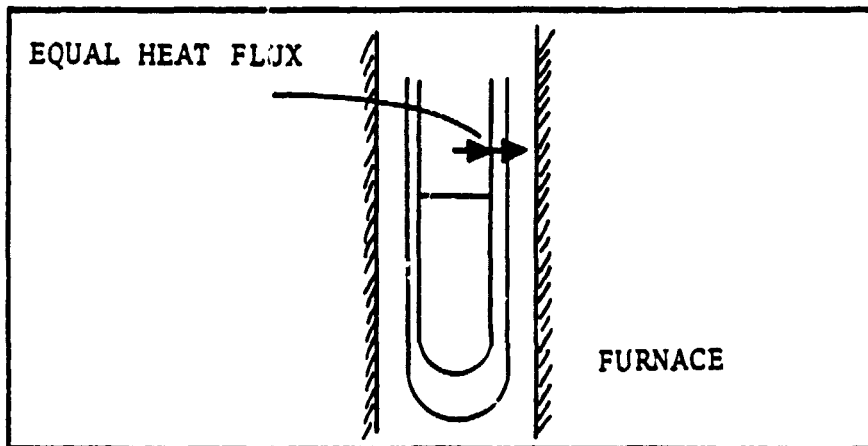


Figure B-4 Heat Conduction Boundary Condition

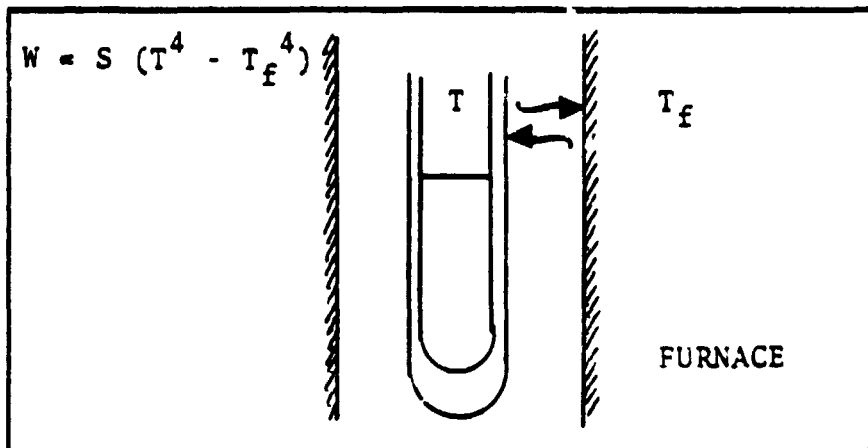


Figure B-5 Radiation Boundary Condition

where k_1 and k_2 are the thermal conductivities on the two sides of the surface, and $(\partial T/\partial n)_i$ represents the thermal gradient normal to the surface in region i . This case might be appropriate for the molten material in contact with the crucible wall (Figure B-4), where

$$k_q \left. \frac{\partial T}{\partial r} \right|_q = k_l \left. \frac{\partial T}{\partial r} \right|_l$$

with subscript q referring to values in the crucible and l referring to values in the molten liquid.

● Radiation -- Liquid/Solid surface in contact with a transparent medium.

Such a boundary condition transfers heat by radiation as well as vapor conduction. An example of this boundary condition is the coupling between the exterior of a crucible and the interior of a furnace (Figure B-5). This radiation flux takes the form $S(T_1^4 - T_2^4)$, where T_1 and T_2 are the temperatures of the two radiating surfaces (i.e., the two surfaces coupled by the transparent medium). The radiation factor S for the B-S thermal problem includes the emissivities of the two surfaces, Boltzman's Constant and a transparency fraction for blackbody radiation from a temperature source. These factors will be described more fully in following discussions relating to the radiative boundary conditions specific to the Bridgman-Stockbarger growth configuration.

Using these classes of boundary conditions, the Bridgman-Stockbarger growth configuration can be completely defined in conjunction with the differential equation (2). Consider, for example, the upper half of the system, i.e., the flow of heat to the melt from the heater. The following is happening:

- 1) Heat is transferred directly from the heater to the melt by radiation from the heater in those wavelengths for which the silica is transparent.
- 2) Heat is transferred to the silica outer surface from the furnace in those wavelengths for which the silica is opaque.
- 3) Heat is transferred from the heater to the gas (if any) by conduction. The gas is considered transparent at all

wavelengths.

- 4) Heat is transferred to the silica from the gas by conduction.
- 5) Heat is transferred to the melt from the quartz by conduction. (This transfer may go the other way if the gas is cooled so that heat is conducted from hot melt to cool silica to cold gas.)
- 6) Heat is radiated to the furnace by the melt at those wavelengths for which the silica is transparent.
- 7) Heat is radiated from the ampoule to the furnace at those wavelengths for which the silica is opaque.

Schematically, these transfer processes are depicted in Figure B-6. The specified boundary conditions for this B-S configuration which relate to these processes are detailed in the following paragraphs.

B.3.1 Solid-Liquid Interface

The solid-liquid interface in the B-S configuration is a conduction boundary condition in which, for every ij node along the interface,

$$k_s \left. \frac{\partial \phi}{\partial z} \right|_{i,j} = k_l \left. \frac{\partial \phi}{\partial z} \right|_{i,j}$$

For this study, we have assumed no radial heat flow along the interface; the impact of this assumption is subject for further analysis.

This boundary condition can easily be expressed in the finite difference format such that ϕ_{ij} on the interface can be computed from its neighboring ϕ_{ij} values. Specifically, for any value of i,

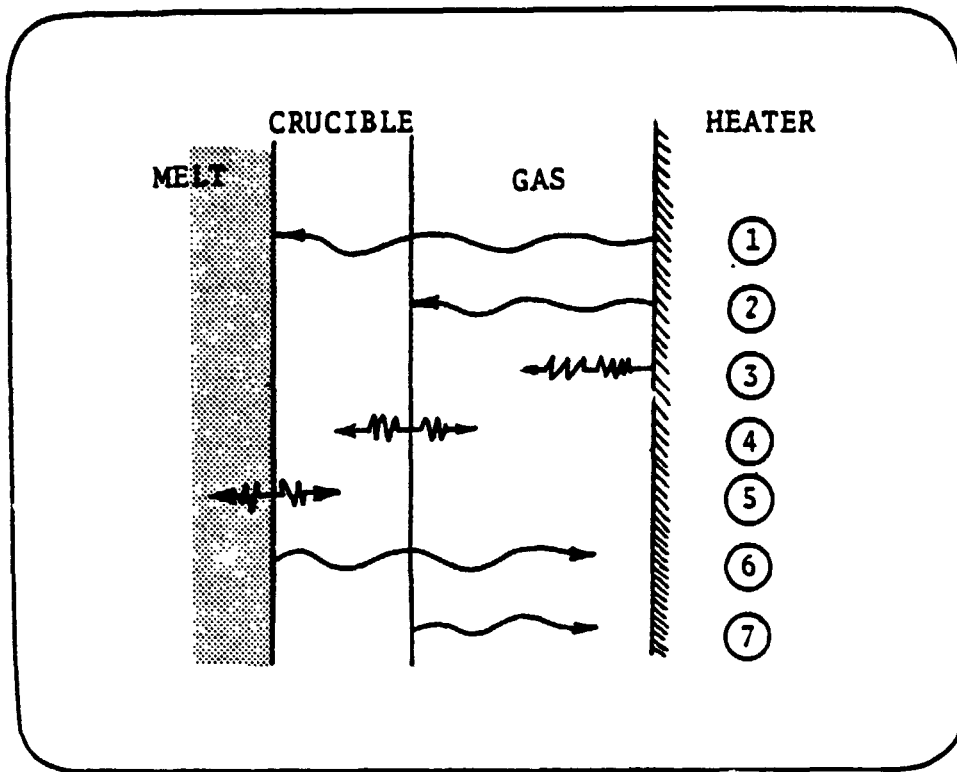


Figure B-6 Schematic Heat Transfer Processes within the B-S Configuration

$$k_s \left[\frac{\phi_{i,j} - \phi_{i,j+1}}{\delta} \right] = k_l \left[\frac{\phi_{i,j-1} - \phi_{i,j}}{\delta} \right]$$

or

$$\phi_{i,j} = \frac{k_l \phi_{i,j-1} + k_s \phi_{i,j+1}}{k_s + k_l} \quad (8)$$

for $j = j^*$ at the solid-liquid interface.

B.3.2 Sample/Crucible Interface (Sample Outer Surface).

Heat flow to and from this interface is both conductive and radiative in nature. Conductive heat transfer occurs between the sample (either solid or melt) and the crucible. Radiative heat flow from the sample surface, and toward this surface from the furnace wall, is also introduced through the crucible because of the transparency of the fused silica to shorter wavelength ($< 3.5\mu$) radiation. The boundary conditions for this interface then are

Liquid-Crucible

$$k_l \left. \frac{\partial \phi}{\partial r} \right|_{i,j} = k_c \left. \frac{\partial \phi}{\partial r} \right|_{i,j} + \epsilon_l \epsilon_h \sigma \left[f_h T_h^4 - f_l T_l^4 \right]$$

Solid-Crucible

$$k_s \left. \frac{\partial \phi}{\partial r} \right|_{i,j} = k_c \left. \frac{\partial \phi}{\partial r} \right|_{i,j} + \epsilon_s \epsilon_e \sigma \left[f_e T_e^4 - f_s T_s^4 \right]$$

where k is the thermal conductivity, ϵ is the emissivity of the radiating surface, σ is the Stefan-Boltzmann Constant, T is the temperature of the radiation source, and f_x is the transparency

fraction for black body radiation from a source at temperature T_x . In these equations, the subscript l represents melt, c = crucible, h = heater, s = solid, and e = extractor. It should be clear that in these boundary condition equations, the temperature terms T_x^4 can be expressed in terms of ϕ_{ij} through the normalizing relationship

$$T_x = (T_{HOT} - T_{COOL}) \phi_{i,j} + T_{COOL} \text{ (}^\circ\text{K)}$$

The above equations can also be represented in the finite difference format such that ϕ_{ij} at this interface can be solved explicitly. However, in addition to ensuring that heat flow in the radial direction is governed by these conditions, conservation of energy dictates that axial conduction effects also be included. Thus for the sample/crucible interface we have the following conditions:

Liquid-Crucible:

$$k_l \left[\frac{\phi_{i,j} - \phi_{i-1,j}}{\delta} \right] = k_c \left[\frac{\phi_{i+1,j} - \phi_{i,j}}{\delta} \right] + \epsilon_l \epsilon_h \sigma \left[f_h T_h^4 - f_l T_l^4 \right] \\ + \left[\frac{k_l + k_c}{2\delta} \right] (\phi_{i,j+1} - \phi_{i,j}) - \left[\frac{k_l + k_c}{2\delta} \right] (\phi_{i,j} - \phi_{i,j-1})$$

or

$$2(k_l + k_c) \phi_{i,j} = k_c \phi_{i+1,j} + k_l \phi_{i-1,j} + \left[\frac{k_l + k_c}{2} \right] (\phi_{i,j+1} + \phi_{i,j-1}) \\ + \epsilon_l \epsilon_h \sigma \left[f_h T_h^4 - f_l T_l^4 \right] \quad (9)$$

where $T_l = (T_{HOT} - T_{COOL}) \phi_{i,j} + T_{COOL}$,

and $T_h = (T_{HOT} - T_{COOL}) \phi_{WALL,j} + T_{COOL}$ ($\phi_{WALL,j}$ is specified).

Solid-Crucible:

$$2(k_s + k_c) \phi_{i,j} = k_c \phi_{i+1,j} + k_s \phi_{i-1,j} + \left[\frac{k_s + k_c}{2} \right] (\phi_{i,j+1} + \phi_{i,j-1}) + \epsilon_s \epsilon_e \sigma \left[f_e T_e^4 - f_s T_s^4 \right] \quad (10)$$

where T_s and T_e are calculated like T_l and T_h , respectively.

Both equations (9) and (10) represent quartic equations in $\phi_{i,j}$ and, as such, can be solved via the Newton-Raphson technique (or equivalent) to obtain $\phi_{i,j}$ at this interface based on the temperatures of the neighboring nodes and the inner furnace wall.

More needs to be said about the transparency function f_x which appears in the radiative terms of these boundary conditions. As these equations indicate, heat is transferred directly from the heater to the melt in the Bridgman-Stockbarger configuration by radiation from the heater in those wavelengths for which the silica is transparent. For these same wavelengths, heat is radiated to the furnace by the melt. In addition, the furnace transfers heat to the silica outer surface in those wavelengths for which silica is opaque, and likewise receives radiated heat from the ampoule in these longer wavelengths.

Black body radiation intensity, W , varies with wavelength and temperature as indicated in Figure B-7. As the figure indicates, the fraction of black body radiated power at wavelengths shorter than λ , can be expressed as

$$f = \frac{\int_0^\lambda W d\lambda}{\int_0^\infty W d\lambda} \quad (11)$$

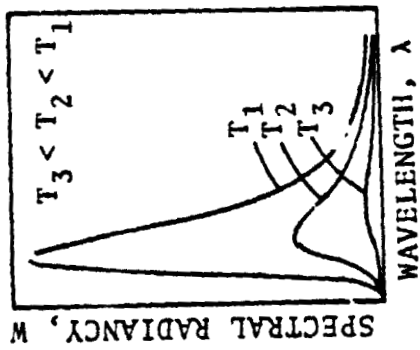


Figure B-7 Spectral Radiance Behavior as a Function of Wavelength and Temperature

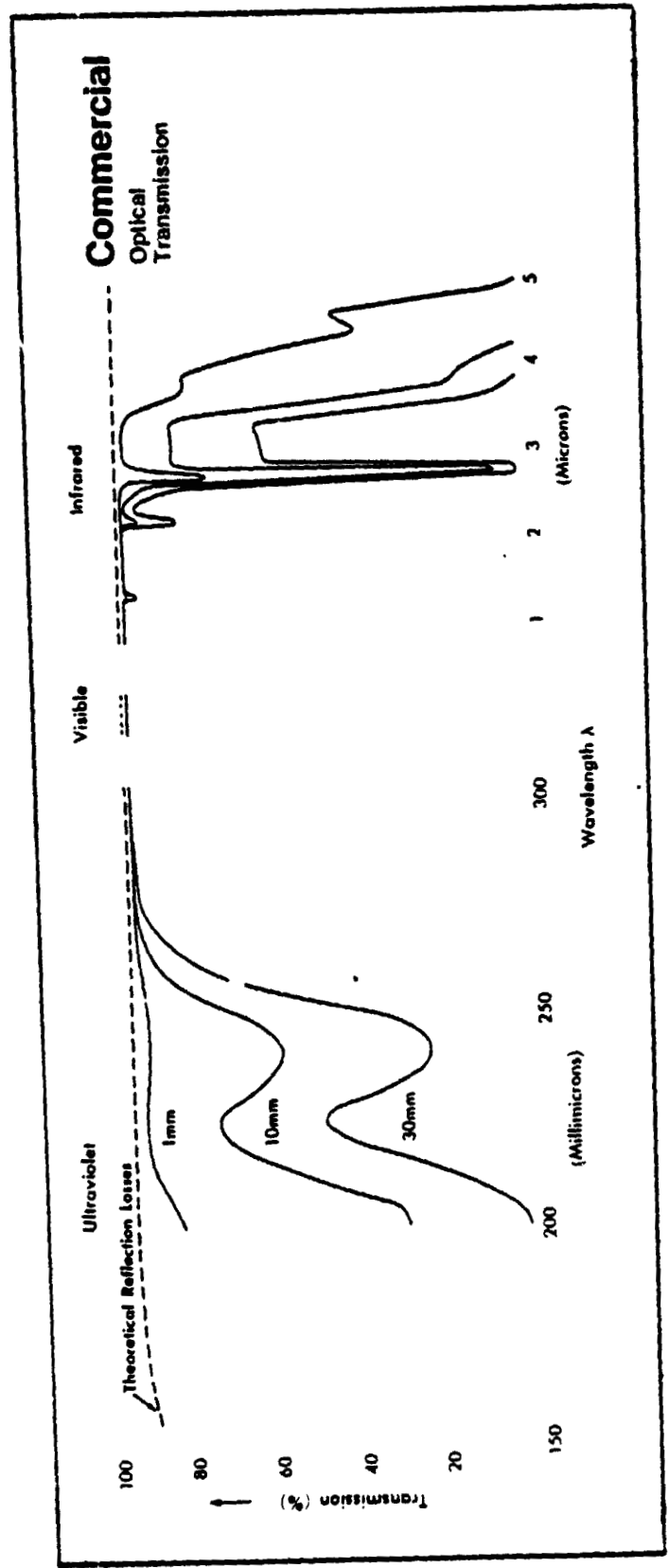


Figure B-8 Fused Silica Optical Transmission Characteristics

The American Institute of Physics Handbook² chapter on radiometry (Table 6k-1, Black-Body Radiation Functions) expresses this fraction f for various values of λT , where T is temperature in degrees Kelvin. The first radiation integral of the A.I.P. table is $f = 1.3 \times 10^{-9}$ for $\lambda T = 0.050 \text{ cm } ^\circ\text{K}$ or $500\mu \text{ } ^\circ\text{K}$. From the optical transmission characteristics of commercial grade fused silica presented in Figure B-8, if the ultra-violet cutoff of radiation is taken to be 0.2μ , virtually total transmission is ensured for $T = 2500^\circ\text{K}$ -- close to the maximum available output with tungsten heaters. At 3600°K and 0.2μ , $T = 720\mu \text{ } ^\circ\text{K} = 0.072 \text{ cm } ^\circ\text{K}$ and $f = 3.2 \times 10^{-4}$, less than 0.032%. Therefore, at reasonable temperatures there is no significant ultraviolet cutoff of black body radiation, and only infrared screening need be considered.

From Figure B-8, we can assume that in the infrared region, quartz has less than 5% first surface reflection loss and remains perfectly transparent for all wavelengths shorter than approximately 3.7μ . Similarly, we will assume that the crucible will act perfectly opaque (and black) for $\lambda > 3.7\mu$. The fraction of total black body radiated power which is at wavelengths shorter than 3.7μ can be obtained as a function of temperature by adapting Table 6k-1 of the A.I.P. Handbook for fused silica. This is done in Table B.1. For $\lambda = 3.6\mu$ and 3.8μ , the appropriate temperatures T are presented and correlated with f_x , the transparency fraction, for the specified value of λT . Figure B-9 graphically presents this f_x fraction as a function of temperature for the transparent wavelengths. When considering the surface radiation from fused silica, the fraction $1 - f_x$ can be used as an effective total emissivity to a first approximation.

² A.I.P., pp 6-154ff, Table 6k-1

TABLE B.1 FRACTION OF TOTAL BLACK BODY RADIATED POWER
AS A FUNCTION OF TEMPERATURE

λT	$\lambda_0=3.6\mu$ T ⁰ C	$\lambda_0=3.8\mu$ T ⁰ C	Transparency Fraction, f (%)
0.10	4.7	-9.84	0.032
0.12	60.3	42.8	0.215
0.14	115.8	95.4	0.782
0.16	171.4	148.1	1.979
0.18	227.0	200.7	3.946
0.20	282.5	253.3	6.690
0.22	338.1	305.9	10.11
0.24	393.6	358.6	14.05
0.26	449.2	411.2	18.54
0.28	504.7	463.8	22.82
0.30	560.3	516.5	27.36
0.32	615.8	569.1	31.85
0.34	671.4	621.7	36.21
0.36	727.0	674.4	40.40
0.38	782.5	727.0	44.38
0.40	838.1	779.6	48.13
0.42	893.6	832.3	51.64
0.44	949.2	884.9	54.92
0.46	1004.7	937.5	57.96
0.48	1060.3	990.2	60.79
0.50	1115.8	1042.4	63.41
0.52	1171.4	1095.4	65.83
0.54	1227.0	1148.1	68.07
0.56	1282.5	1200.7	70.13
0.58	1338.1	1253.3	72.04
0.60	1393.6	1305.9	73.81
0.62	1449.2	1358.6	75.44
0.64	1504.7	1411.2	76.94

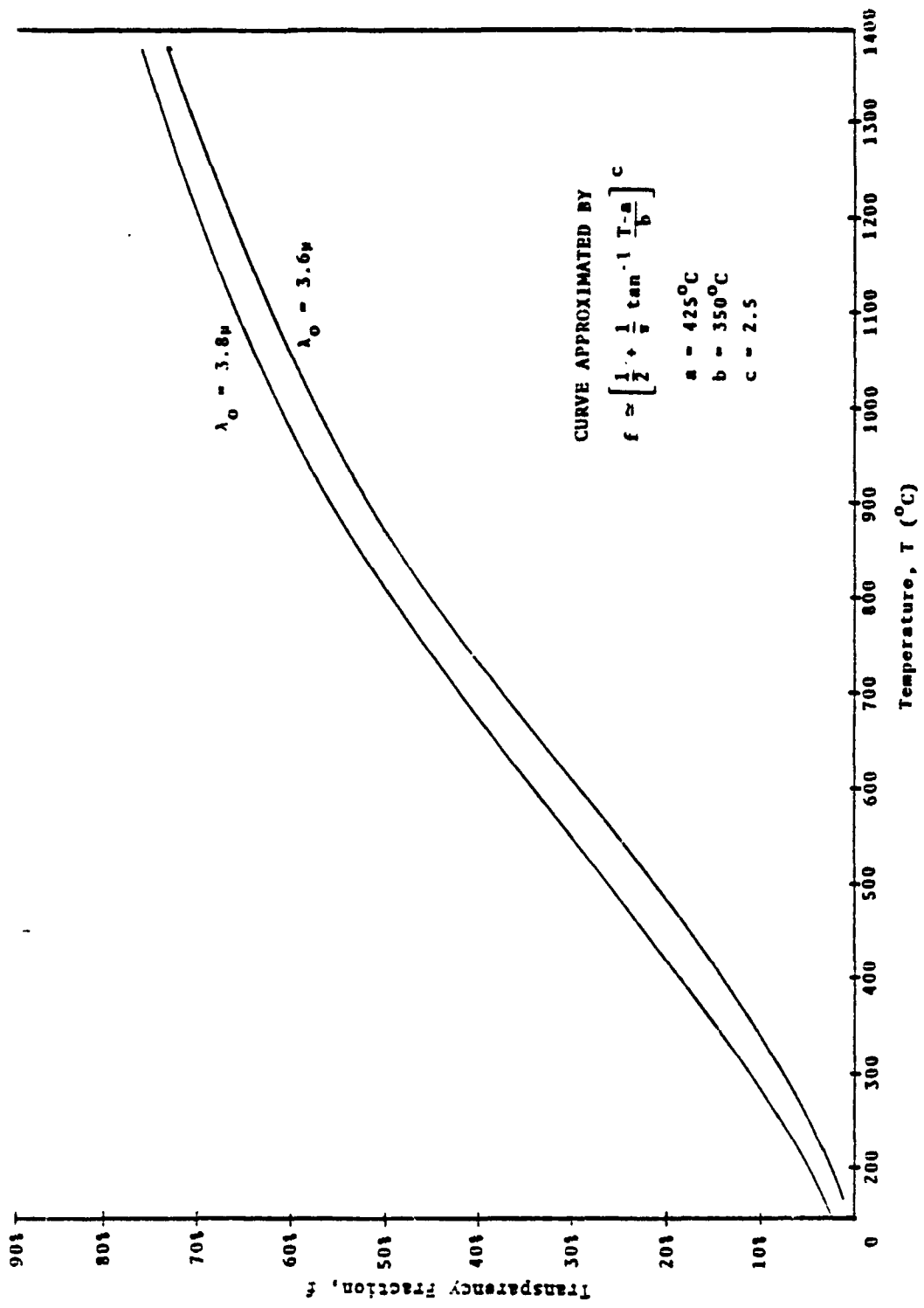


Figure B-9 Fused Silica Transparency Fraction as a Function of Temperature

For purposes of modeling this transparency fraction in our Bridgman-Stockbarger thermal analyses, Figure B-9 may be approximated by analytically-convenient functions. The first function suggested is the straight line

$$f_x = (T - 150^\circ\text{C})/1400^\circ\text{C},$$

which stays within $\pm 3\%$ up to $T = 1075^\circ\text{C}$, but must be adjusted at both low and higher temperatures. A much improved analytic function, which is accurate over a wider range of temperatures (particularly at higher T 's) and has no discontinuities in its derivative, is

$$f_x = \left\{ \frac{1}{2} + \frac{1}{\pi} \tan^{-1} \left(\frac{T - a}{b} \right) \right\}^c \quad (12)$$

This curve has its inflection at $T = a$, $f = 1/2^c$; reasonable values which we have assumed for our thermal models are $a = 425^\circ\text{C}$, $b = 350^\circ\text{C}$, and $C = 2.5$.

B.3.3 Crucible/Furnace Interface (Outer Crucible Wall)

Similar boundary conditions exist at the outer crucible wall as were specified for the inner crucible surface, namely,

Crucible - Heater:

$$k_c \left. \frac{\partial \phi}{\partial r} \right|_{i,j} = k_g \left. \frac{\partial \phi}{\partial r} \right|_{i,j} + \epsilon_c \epsilon_h \sigma \left[(1-f_h) T_h^4 - (1-f_c) T_c^4 \right]$$

Crucible - Extractor:

$$k_c \left. \frac{\partial \phi}{\partial r} \right|_{i,j} = k_g \left. \frac{\partial \phi}{\partial r} \right|_{i,j} + \epsilon_c \epsilon_e \sigma \left[(1-f_e) T_e^4 - (1-f_c) T_c^4 \right]$$

where the subscript g represents the gas surrounding the ampoule (the remaining parameters are defined as before). Naturally, if crystal growth is being accomplished in a vacuum, the conductive term $k_g \frac{\partial \phi}{\partial r}$ becomes zero. Note that for this boundary condition, the energy radiated from the two coupled surfaces is that radiation for which the crucible is not transparent (i.e., the longer wavelengths). That fraction of energy not "passed" through to the ingot is represented by $(1 - f_x)$, the "opaqueness fraction".

The conservation of heat flow expressed by these boundary conditions and the axial conduction along the outer crucible surface allows us to specify the following finite difference expressions for the crucible/furnace interface:

Crucible - Heater:

$$2(k_c + k_g) \phi_{i,j} = k_c \phi_{i-1,j} + k_g \phi_{i+1,j} + \left[\frac{k_c + k_g}{2} \right] (\phi_{i,j+1} + \phi_{i,j-1}) + \epsilon_c \epsilon_h \sigma \left[(1-f_h) T_h^4 - (1-f_c) T_c^4 \right] \quad (13)$$

Crucible - Extractor:

$$2(k_c + k_g)\phi_{i,j} = k_c\phi_{i-1,j} + k_g\phi_{i+1,j} + \left[\frac{k_c + k_g}{2} \right] (\phi_{i,j+1} + \phi_{i,j-1}) + \epsilon_c \epsilon_e \sigma \left[(1-f_e)T_e^4 - (1-f_c)T_c^4 \right] \quad (14)$$

where, in both cases, $T_c = (T_{HOT} - T_{COOL})\phi_{i,j} + T_{COOL}$

The same transparency function f_x (as a function of T_x) which was described in Section B.3.2 is utilized in these equations to establish the fraction of energy radiated to and from this boundary -- indicating the degree of opaqueness of the crucible at these temperatures. Again, if the ampoule is in a vacuum ($k_g = 0.$), these equations are simplified somewhat.

B.3.4 Inner Furnace Wall

As mentioned previously, the purpose of this study was not to address particular furnace designs, but to determine optimum ampoule thermal conditions and establish the associated furnace specifications. In this regard, of primary importance is the analysis of the inner furnace wall temperature profile and the resulting thermal coupling effects with the outer crucible wall.

To assist in this analysis, an input temperature profile model was developed to facilitate parametric evaluations of several furnace configurations representing external temperature sources to the B-S system. The intent of this model was to provide an input temperature profile (normalized) along the inner wall as a

function of distance away from the solid/liquid interface, $\phi = f(z)$, for both the hot and cold ends. The form of this model is

$$\phi_{\text{WALL}} = 1. + A e^{Bz} \quad \text{for } z < 0 \quad (\text{hot end}) \quad (15)$$

$$\phi_{\text{WALL}} = C e^{-Dz} \quad \text{for } z > 0 \quad (\text{cool end}) \quad (16)$$

with the constants A, B, C and D positive numbers. By judiciously controlling these input parameters, the inner wall profile can be adjusted to represent several furnace configurations. For example, if a constant temperature surface is required at both the hot and cool ends, $B = D = 0$, and C and A are adjusted to create the desired normalized temperatures for all z's. Temperature profiles also can be produced which decay exponentially from T_{MAX} at the solid/melt interface to a steady-state temperature a specified distance away from the interface. The analysis of such profiles determines the thermal gradient payoff achieved by using a furnace with a temperature boost capability near the heater-cooler interface. Note that the temperature profiles on each side of the liquid-solid interface can be controlled independently.

The specified inner wall temperature profile represents an external heat source (and sink) which becomes a boundary condition for the Bridgman-Stockbarger configuration. Where practical, it is desirable to select the finite difference grid system such that this boundary (and all boundaries) is represented by a set of node points within this grid.

B.4 ITERATIVE PROCEDURE AND ACCURACY

Several procedures exist for solving the system of finite difference equations with the appropriate boundary conditions. For steady state problems, the relaxation process is usually superior. Utilizing the correct established relationship (either equations (6) and (7) for internal grid points, or the appropriate boundary condition equation for a boundary node point (8) - (10), (13) - (16) , a temperature can be systematically calculated for every node point ij based on the temperature of the neighboring nodes. After a value of $\phi_{i,j}$ is calculated for each node point in the system, successive iterations are performed for the entire grid until convergence is achieved. For the physical problem at hand, convergence can be formulated by examining the change in the ϕ_{ij} values on successive iterations, requiring that $|\phi_{ijNEW} - \phi_{ijOLD}| < \epsilon_0$.

The accuracy, stability, and time of convergence of this iterative technique in practice depends on the particular boundary conditions (i.e., configurations) imposed. This study included a parametric variation of ϵ_0 to establish the sensitivity and range of temperature accuracies, and the corresponding variation in number of cycles required for convergence. We have also analyzed several techniques to improve convergence including

- using only values from the preceding iteration for all neighboring node temperatures
- incorporating all new (i.e., from the current iteration) node temperatures into the calculations whenever possible
- providing better initialization values for the grid network. For example, initial values of the system thermal profiles

are better represented by an arc tangent function (as a function of axial distance from the solid-liquid interface) than being constant throughout the hot and cold ends. Similarly, when successive parametric cases are being executed, the solution to one case provides an excellent initialization network for the calculations of the next case.

This study has identified other iterative methods for solving the system of finite difference equations presented for the Bridgman-Stockbarger configuration, with potential to improve the rapidity and accuracy of convergence. We recommend that future thermal analysis efforts using the finite difference techniques and computer model developed during this study address these possible enhancements.